

NAM

Impact of Production Fluctuations on Groningen Seismicity

Geomechanical Modelling using Rate and State friction

ExxonMobil Upstream Research Company

Nora DeDontney and Suvrat Lele

Date October 2018

Editors Jan van Elk & Dirk Doornhof

General Introduction

The seismological model (Version 5) currently used in the assessment of hazard and risk for the induced seismicity in Groningen, provides a probabilistic prediction of the seismicity dependent on the local reservoir pressure depletion associated with the gas volume produced. The seismicity is in this model not dependent on the gas production rate. The gas volume extracted determines reservoir pressure depletion, which governs the expected number and magnitude of induced earthquakes. Within the model, the expected number of events depends on the pressure depletion, but not the rate of that depletion. Theoretically, there are processes which potentially could cause the expected event number, for a given incremental volume of gas production to depend on the rate of that gas production. These could be associated with the geomechanical behaviour of faults (e.g. rate and state frictional fault behaviour) or compaction (e.g. a-seismic stress relaxation at production time scales).

However, studies carried out as part of the research program of NAM have not been able to identify whether these processes play a significant role or been able to quantify the impact of gas production rate on seismicity. In an environment of decreasing and more stable gas production rates, ignoring potential production rate dependency of the seismicity will be conservative and lead to a potential over-estimation of hazard and risk.

Given the current state of knowledge, NAM is not in a position to increase the sensitivity of the seismological model to production rate changes as this was so far found to degrade the performance of the model and accepts that as a result the assessment of hazard and risk might be conservative. The current model yields a sensitivity to seasonal depletion rate changes that is thought to be close to the upper bound of sensitivities consistent with the observed catalogue. On the other hand, based on the research to date, seasonal seismicity variations within the catalogue are lower than the detection threshold.

In the operation of the field, NAM will make every effort to reduce fluctuations in gas production. The Minister of Economic Affairs has, on the advice of the regulator SodM, imposed limits to the production fluctuations. NAM will report on any excursions from these set limits.

In recent years, NAM has carried out several studies into the dependency of the induced seismicity in Groningen on the gas production rate from the field. This included studies into reservoir behaviour (Ref. 1), modelling of the various mechanisms that could induce production rate dependency (Ref. 4) and analysis of field data using machine-learning (Ref. 6) and statistical techniques (Ref. 2, 3, 4 and 5).

This report describes a new geomechanical model to generate (simulated) sequences of earthquakes by implementing a new rate and state friction description of the fault behavior and to investigate whether this mechanism induces production rate dependency.

References

1. Geurtsen, L., P. Valvatne and A. Mar-Or, Optimisation of the Production Distribution over the Groningen field to reduce Seismicity, NAM, December 2017
2. Bierman S.M., R. Paleja, and M. Jones, Statistical methodology for investigating seasonal variation in rates of earthquake occurrence in the Groningen field, January 2016
3. Bierman S.M., Seasonal variation in rates of earthquake occurrences in the Groningen field, August 2017
4. Bourne, Stephen and Steve Oates, The influence of stress rates on induced seismicity rates within the Groningen field, Shell Research, August 2018.
5. Burch D. and B. Symington, Impact of Production Fluctuations on Groningen Seismicity – Part 2, Data Analytics, ExxonMobil Upstream Research Company, 2018.
6. Park T., H. Jamali-Rad, W. Oosterbosch, J. Limbeck, F. Lanz, C. Harris, E. Barbaro, K. Bisdom & K. Nevenzeel, Seasonality analysis for induced seismicity event rate time series within the Groningen Field, Shell Research and IBM, August 2018.



NAM

Title	Impact of Production Fluctuations on Groningen Seismicity Geomechanical Modelling using Rate and State friction		Date	October 2018
			Initiator	NAM
Autor(s)	Nora DeDontney and Suvrat Lele	Editors	Jan van Elk and Dirk Doornhof	
Organisation	ExxonMobil Upstream Research Company	Organisation	NAM	
Place in the Study and Data Acquisition Plan	<p>The seismological model (Version 5) currently used in the assessment of hazard and risk for the induced seismicity in Groningen, provides a probabilistic prediction of the seismicity dependent on the local reservoir pressure depletion associated with the gas volume produced. The seismicity is in this model not dependent on the gas production rate. The gas volume extracted determines reservoir pressure depletion, which governs the expected number and magnitude of induced earthquakes. Within the model, the expected number of events depends on the pressure depletion, but not the rate of that depletion. Theoretically, there are processes which potentially could cause the expected event number, for a given incremental volume of gas production to depend on the rate of that gas production. These could be associated with the geomechanical behaviour of faults (e.g. rate and state frictional fault behaviour) or compaction (e.g. a-seismic stress relaxation at production time scales).</p> <p>However, studies carried out as part of the research program of NAM have not been able to identify whether these processes play a significant role or been able to quantify the impact of gas production rate on seismicity. In an environment of decreasing and more stable gas production rates, ignoring potential production rate dependency of the seismicity will be conservative and lead to a potential over-estimation of hazard and risk.</p> <p>Given the current state of knowledge, NAM is not in a position to increase the sensitivity of the seismological model to production rate changes as this was so far found to degrade the performance of the model and accepts that as a result the assessment of hazard and risk might be conservative. The current model yields a sensitivity to seasonal depletion rate changes that is thought to be close to the upper bound of sensitivities consistent with the observed catalogue. On the other hand, based on the research to date, seasonal seismicity variations within the catalogue are lower than the detection threshold.</p> <p>In the operation of the field, NAM will make every effort to reduce fluctuations in gas production. The Minister of Economic Affairs has, on the advice of the regulator SodM, imposed limits to the production fluctuations. NAM will report on any excursions from these set limits.</p>			

	<p>In recent years, NAM has carried out several studies into the dependency of the induced seismicity in Groningen on the gas production rate from the field. This included studies into reservoir behaviour, modelling of the various mechanisms that could induce production rate dependency and analysis of field data using machine-learning and statistical techniques.</p> <p>This report describes a new geomechanical model to generate (simulated) sequences of earthquakes by implementing a new rate and state friction description of the fault behavior and to investigate whether this mechanism induces production rate dependency.</p>
Directly linked research	<ul style="list-style-type: none"> (1) Gas Production (2) Reservoir Modelling (3) Geomechanical Modelling (4) Seismological Model
Used data	
Associated organisation	NAM
Assurance	

Impact of Production Fluctuations on Groningen Seismicity – Part 1

Geomechanical Modelling using Rate and State friction

ExxonMobil Upstream Research Company

Nora DeDontney and Suvrat Lele

Table of Contents

0.0	Executive Summary.....	2
1.0	Overview of Studies	4
2.0	Analytical Reservoir Pressure Modeling	7
2.1	Introduction and Model Setup.....	7
2.2	Results of Analytical Model.....	10
2.3	Summary and Conclusions.....	16
3.0	Geomechanical Modeling of Earthquake Cycles.....	17
3.1	Introduction to Rate and State Friction	17
3.2	Earthquake Activity Rate Models.....	20
3.2.1	Activity Rate Model Background.....	20
3.2.2	Activity Rate Model Parameters	21
3.2.3	Activity Rate Results.....	23
3.2.4	Detection of Earthquake Seasonality with Simulated Earthquake Catalogs	26
3.2.5	Activity Rate Conclusions	27
3.3	Earthquake Cycle Models.....	27
3.3.1	Earthquake Cycle Model Setup.....	28
3.3.2	Earthquake Cycle Model Results.....	37
3.3.3	Earthquake Cycle Model Conclusions	52
3.4	Geomechanical Modeling Summary and Conclusions.....	53
4.0	Alternate Lines of Investigation	55
4.1	Static Coulomb Friction Models.....	55
4.1.1	Introduction and Model Setup.....	55
4.1.2	Static Model Results.....	57
4.1.3	Summary and Conclusions	58
4.2	Surface Reservoir Water Level Fluctuations as an Analog.....	59
5.0	Summary and Conclusions	60
	References	62

0.0 Executive Summary

The Groningen field has long been produced with fluctuations in production rate over a range of time scales. Daily fluctuations occur at individual wellheads as maintenance is performed, as daily demand changes or as production is shifted. Seasonal fluctuations occurred due to the high winter production required to meet demand during the cold winter months. Fluctuations over the decade timescale occur in response to the market or to changes in infrastructure. The occurrence of seismicity over the last 20 years has raised the question of whether fluctuations in production result in a different seismic catalog than a constant rate of production would produce. By understanding if production fluctuations can alter the character the seismicity it may be possible to provide insight into an optimal production strategy to manage the seismicity.

ExxonMobil Upstream Research Company (EMURC) has addressed this question by attempting to determine if fluctuations in production would increase the seismic hazard compared to a constant production scenario (here hazard is defined qualitatively as resulting in more or bigger earthquakes over a time frame, not defined by a peak ground acceleration with a specified probability of exceedance). EMURC performed a preliminary investigation using tools available on-hand or that could be quickly developed. The study examined the pore pressure history at various distances from a fault due to fluctuating production, the predicted activity rate changes that would occur due to variations in loading rate and the energy dissipated by fault slip in a 3D geomechanical model for different scenarios. Some of these tools provided insightful results, some were simple and in need of expansion and some were not well-suited to address the question. Further work was identified and led to a more comprehensive study.

This study had two areas of focus: 1) the development and use of a new geomechanical model to generate simulated sequences of earthquakes by implementing a new frictional description of the fault, and 2) a statistical analysis of the historical Groningen production schedule and observed earthquake behavior to determine if there is any evidence that production fluctuations affect seismicity. The results from these two recent studies, as well as the early preliminary work, are presented here.

The newly developed geomechanical model simulates both the coseismic (during an earthquake) and interseismic (between earthquakes) times and generates a synthetic earthquake catalog dependent on a random initial stress condition on the fault. Many catalogs are simulated under different loading histories and the results are examined in aggregate to determine if there is a statistically significant effect on the observed seismicity. Many parameters and forms of implementation are examined and no model identified a change in the character of the modeled seismicity as a result of different loading histories. This model does not show that aggregate seismic hazard should be affected by fluctuations in production and to date, no physical model has been identified to support the hypothesis that fluctuations in production alter the seismic hazard. The production schedule does affect the timing of modeled earthquake events but it is the total volume of gas produced that controls the moment release, and hence the hazard. For example, the model shows that if a given amount of gas is produced each year, shifting more production to the winter increases the number of events in the winter and spring but statistically the same modeled number and magnitude of events occur during the year as if the production had been

constant throughout the year. Therefore, since there is no change in the total number of events or the expected magnitudes, the model implies no change in the aggregate hazard for the year.

It is possible that a physical model could be found in the future that links fluctuations in production to increased hazard, but the basis of that model is not currently known to EMURC.

1.0 Overview of Studies

It has been fully recognized that gas production and pressure depletion of the Groningen Gas Field induces seismicity in the Groningen area. As of Jan 1 2017, 286 earthquakes with a moment magnitude of 1.5 or greater have been recorded in the area. It has also been noted that when looking at the entire catalog of Groningen earthquakes (with magnitudes down to as low as -0.2), a seasonality in the rate of occurrence of seismic events is suggested (blue bars in Figure 1). Because the earthquake catalog is complete only down to magnitude 1.5, the suggested seasonality is often considered “suspected” rather than “proven” because the seasonal trend is not apparent when only magnitude ≥ 1.5 events are examined (red bars in Figure 1).

Many studies have focused on determining if the “suspected” seasonality is real (Bierman et al., 2015 and Nepveu, et al., 2016) but have not addressed whether seasonality or other production fluctuations affects the hazard posed to the population. It is natural to question if variable or “swing” production, whether seasonal or even daily in frequency, impacts the aggregate seismic hazard posed by producing gas from Groningen. “Aggregate” seismic hazard is here defined qualitatively by the number of events and the size of events over a time frame that is long with respect to the frequency of variable production (the hazard is increased if more events are expected or if larger events are expected). If a one year time frame is considered, shifting earthquakes from the summer to winter months does not affect the hazard because the same number of events would be expected over a one year period.

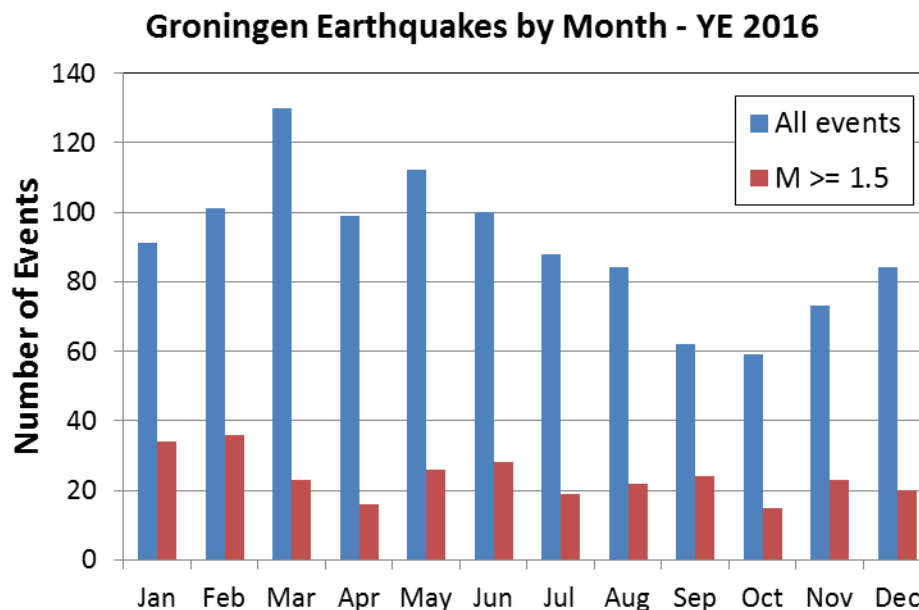


Figure 1: Groningen earthquakes by month. Suspected seasonality is apparent when looking at the entire catalog, but not when considering only the complete catalog ($M \geq 1.5$).

Hazard is affected by the number of events expected to occur over a time period and the character of the seismicity as described by the Gutenberg-Richter b-value (Gutenberg and Richter, 1954). The b-value characterizes the relative abundance of small versus large events. If the same seismic moment is released via an earthquake catalog with a low b-value vs. a high b-value, the low b-value catalog will have more

large earthquakes and fewer small magnitude events. If a fixed number of earthquakes occur in a year, a low b-value year will have more large earthquakes. No matter the constraint applied, moment release or number of events, a low b-value catalog will increase the resulting seismic hazard because more frequent large, and potentially damaging, events would be expected to occur.

In light of this, the important question for Groningen seismicity is not if there are more earthquakes during times of high production, but whether the character of the seismicity is changed by the swings in production. The key question is:

If a given amount of gas is produced from Groningen in a year, is the expected number or b-value of earthquakes in that year influenced by whether the production was steady (constant rate), or variable (on daily, monthly, or seasonal frequencies)?

As a well experiences highs and lows in production, the pore pressure field around the well changes. Analytical models of reservoir pressure near a producing well were used to estimate the pore pressure evolution occurring as a result of the drawdown around a well with variable production over a range of time and length scales. The models indicate that even very close to the well, local drawdowns are quite small compared to the general reservoir depletion at Groningen for daily or seasonal swings in production. Pore pressures can increase or decrease in the immediate vicinity of a well due to variable production but most of the field will follow a monotonically decreasing pore pressure trend and will not feel any effects from variations in production rate. The minimal effect on the pore pressure field suggests that fluctuations should have no influence on overall earthquake occurrence rate or magnitude because most faults in the field are unaffected by whether wells are producing at a constant rate or are fluctuating in production.

While the effect of fluctuations on faults is calculated to be small, geomechanical models can be used to examine if the effect is large enough to result in a change in earthquake character. They can also test for the effect of large variations in stressing histories in the event that the pore pressure effect on the fault is larger than anticipated. Geomechanical models that incorporate a path (or history) effect are necessary to evaluate the effect of production fluctuations on the resulting earthquake catalog. Models where the fault surface interaction is governed by rate-and-state friction, rather than Coulomb friction, are able to account for a history effect. The simplest implementation of this law examines that effect of the stress history on the number of earthquakes and does not account for earthquake magnitude. The model imposes a background stressing rate and variable production is simulated by making changes to the background stressing rate. For reasonable choices of model parameters at Groningen, the cumulative number of earthquakes is found to be dependent only on the average background stressing rate over time and is insensitive to how the stressing rate is distributed throughout the year. This model result leads to the conclusion that the cumulative number of earthquakes (and hence the aggregate seismic hazard) is not impacted by variable versus steady production.

To fully capture the problem, earthquake magnitudes, and not just numbers of events, must be accounted for by solving the rate-and-state equations over a model domain. Rather than a steady-state accumulation of slip (as is modeled in a quasi-static finite element model), a quasi-dynamic model is able

to have discrete earthquake events over subsets of the model domain and capture the effect of the stress history during the interseismic time. The result is an earthquake cycle model that generates a catalog of earthquakes over time, not just one, slow event. Physical models like this determine the effect of various parameters on the catalog, and are necessary to be able to forecast the effect on seismicity for different production scenarios. When exposed to different stress histories, the same realization of initial conditions can result in different earthquake catalogs due to the incorporated history dependence. Some simulated catalogs can have more big earthquakes when following the constant production stress path and some can have more big events when following the seasonal swing stress path; however, when a large number of simulated catalogs are viewed in aggregate, there is no difference in the character of the earthquake catalogs for the different stress histories. This means that this physical model does not support the idea that fluctuations in production impact the seismic hazard and should be avoided.

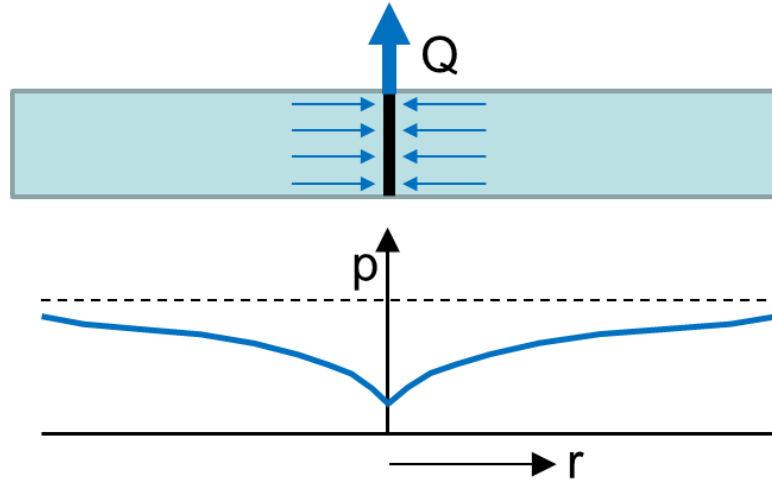
2.0 Analytical Reservoir Pressure Modeling

2.1 Introduction and Model Setup

For fluctuations in production to have an effect on seismicity there must be a method of communicating information about the fluctuations to the seismogenic region of a fault. The most logical choice for this communication pathway is the pore pressure. The time history of the pore pressure evolution at any point in the field is dependent on the production schedule. Additionally, there is a coupling between the pore pressure and the total stress evolution (vertical total stress is unchanged in time but horizontal total stress varies with depletion). By solving for the time and position dependent pore pressure (and therefore stressing) histories, it can be determined if there is a viable pathway for faults to be able to respond to fluctuations in production.

As a well experiences highs and lows in production, the pore pressure field around the well changes. During times of high production, the bottomhole pressure is low so that the large pressure gradient between the reservoir and the wellbore drives a large flux of gas. This low bottomhole pressure translates into a low pore pressure in the immediate vicinity of the well. Alternatively, at times of low production, the pressure gradient is small so the pore pressure in the vicinity of the well is higher than during times of high production. The pressure disturbance due to changes in production is only felt a finite distance from the wellbore and this distance is controlled by the parameters that describe the reservoir and the fluid such as the permeability, gas compressibility and the duration of the production perturbation. The pressure disturbance due to fluctuations in production is not felt far away from the wellbore. At a large enough distance the pore pressure monotonically decreases, but at a non-uniform rate, and at further distances the pore pressure appears to monotonically decrease at a constant rate.

Analytical models of reservoir pressure near a producing well were used to estimate the pore pressure evolution occurring as a result of the drawdown around a well with variable production. These models were constructed, based on a single well in an infinite-acting, compressible gas reservoir. While these calculations are approximate, they should capture the pressure drawdown near wells to first order. The model is illustrated in Figure 2. As shown in the figure, the analytical solution for reservoir pressure utilizes exponential integral functions. A single exponential integral function can be used to model a constant production rate. Variable rates can be simulated by superposing multiple exponential integral solutions.



Reservoir pressure given by:

$$p = p_{init} - \frac{Q\mu}{4\pi kh} \left\{ E_1 \left(\frac{r_w^2}{4\eta t} \right) \right\}$$

Figure 2. Illustration of analytical reservoir fluid flow model.

Rock and fluid flow properties were taken from estimates for the field as a whole and are summarized in Table 1. The average pore pressure in the field is decreasing due to the depletion of the reservoir. However, one particular question of interest is whether the pore pressure is monotonically decreasing across the field or if there are areas where both pore pressure decreases and increases occur due to the production fluctuations. In the case of monotonically decreasing pore pressures the faults in the reservoir are slowly being brought closer and closer to failure but potentially at a non-constant rate. If pore pressure increases occur, the faults are repeatedly being brought towards failure and then away from failure. These differences in the stress path could have implications for the effect on seismicity.

Table 1. Rock and Fluid Flow Properties for Reservoir Modeling. Several of the values used come from the Technical Addendum to the 2013 Winningsplan. The base case properties include a permeability of 150 mD. Lower-perm and higher-perm cases were also run at 50 mD, and 450 mD (3X-higher and 3X-lower).

In order to determine a representative well production rate, a field-wide rate of 35 GNm³/year was assumed. Assuming 297 wells, correcting for the 14% nitrogen in Groningen gas, and estimating the reservoir density of the gas, an average representative well production rate of 32,000 res-bbls/day was estimated. This value was used directly in constant rate calculations and as a long term average value in variable rate calculations. To examine the effect of daily variability in production, an extreme case of 12 hours of no production, and 12 hours of full production (64,000 res-bbls/day for 12 hours) was used. Additionally, a seasonal swing in production was examined with an average rate of 32,000 res-bbls/day

The average pore pressure in the field is decreasing due to the depletion of the reservoir. However, one particular question of interest is whether the pore pressure is monotonically decreasing across the field or if there are areas where both pore pressure decreases and increases occur due to the production fluctuations. In the case of monotonically decreasing pore pressures the faults in the reservoir are slowly being brought closer and closer to failure but potentially at a non-constant rate. If pore pressure increases occur, the faults are repeatedly being brought towards failure and then away from failure. These differences in the stress path could have implications for the effect on seismicity.

Table 1. Rock and Fluid Flow Properties for Reservoir Modeling.

Property	Symbol	Value
Permeability	k	50, 150, 450 mD
Porosity	ϕ	0.12 ⁽¹⁾
Gas Viscosity	μ_g	0.0157 cp
Young's Modulus	E	15 GPa
Poisson Ratio	ν	0.18
Rock Compressibility	C_R	3.62×10^{-6} 1/psi
Gas Compressibility	C_g	7.65×10^{-4} 1/psi
Total Compressibility	C_T	7.69×10^{-4} 1/psi
Diffusivity	η	655,520 ft ² /day
Gas density (standard conditions)	$\rho_{g \text{ (std)}}$	0.000787 g/cc
Gas density (reservoir conditions)	$\rho_{g \text{ (res)}}$	0.0598 g/cc
Production Rate	Q	32000 res-bbls/day
Reservoir Thickness	h	250 meters
Δp scaling	$Q\mu_g/4\pi kh$	0.288 psi
Initial pressure	p_{init}	1377.86 psi
Reservoir temperature	T_r	100 °C
⁽¹⁾ – Reflects gas-filled porosity		

2.2 Results of Analytical Model

The amount of pore pressure variation is highly dependent on the reservoir permeability. Figure 3 illustrates the pore pressure histories, at various distances from the wellbore, for three different permeabilities, in the case of extreme daily fluctuations of 12 hours on and 12 hours off. In the case of a low permeability, it takes a long time for the pressure signal to migrate from the well, so the result is large swings in the proximal pore pressure as the effect is unable to leave the vicinity of the wellbore. For high permeabilities, the pressure signal travels rapidly and the proximal pore pressure history has only small swings.

Even for the extreme case of on for 12 hours and off for 12 hours, none of the cases predict a significant effect of variable production on pore pressure at a distance of 300 meters from the well. For the low permeability case, the pore pressure is monotonically decreasing and for the high permeability case, the pressure swing is less than ± 0.007 bar. At 100 meters from the well there is a pressure swing ± 0.04 bar for the low permeability case. At 8 meters from the well the maximum daily pressure swing in this case is ± 0.32 bar. For the base case permeability, the corresponding number is ± 0.12 bar. These variations are all very small compared to the 200 bar of depletion that has already occurred in the field.

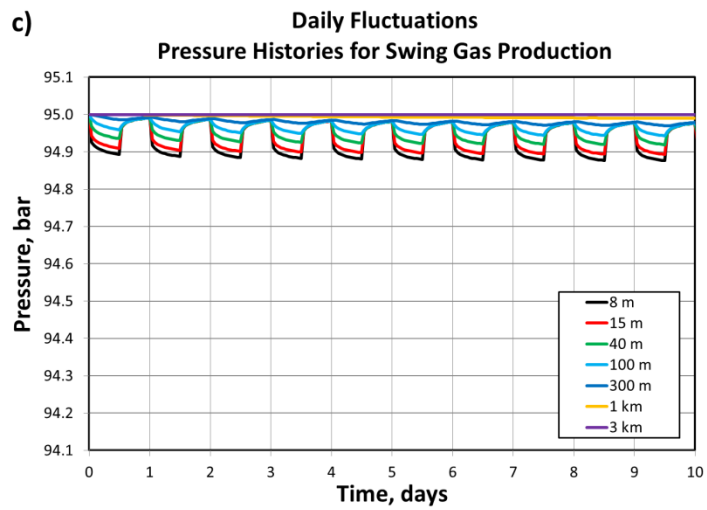
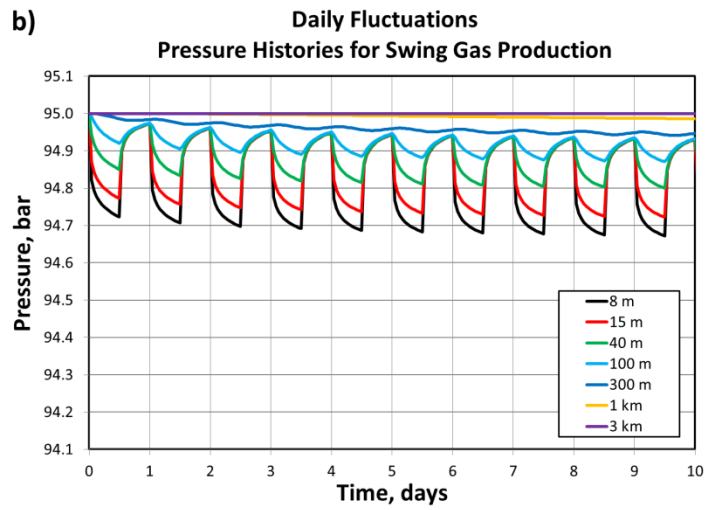
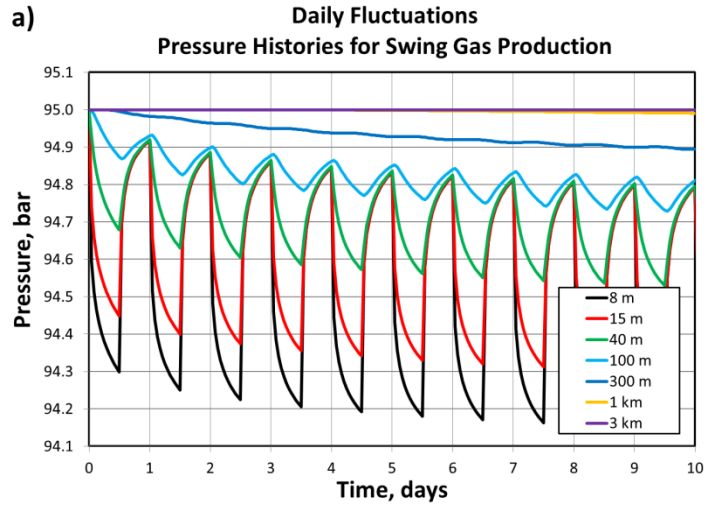


Figure 3. Pressure histories at various distances from a well with daily production variations for three permeability cases: a) low permeability of 50 mD, b) base case permeability of 150 mD and c) high permeability of 450 mD.

In reality, the daily production swings at Groningen are not nearly as severe as 12 hours on and 12 hours off ($\pm 100\%$). Figure 4 shows eight weeks of production rate data for February-March of 2013. The daily production fluctuation can be seen to be $\sim \pm 10\%$ so the results shown in **Error! Reference source not found.** are an extreme upper bound to the pore pressure changes that should be felt in around the wellbore, related to daily production rate variability.

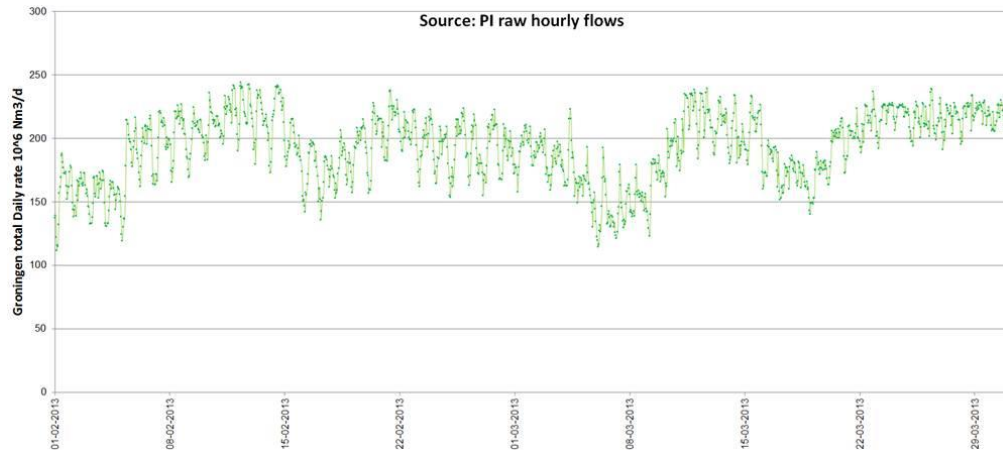


Figure 4. Groningen production data, reflecting daily production swings of approximately $\pm 10\%$.

A similar analysis was conducted to examine the effect of the production fluctuations on a seasonal or yearly time scale as implemented prior to 2015. A set of monthly gas production rates was imposed, designed to be representative of the actual seasonal fluctuations. The imposed rates are illustrated in Figure 5. Groningen field production data showing the actual seasonal fluctuations over multiple years are displayed in Figure 6.

The results of the calculation are shown in Figure 7 for the base case permeability of 150 mD. Nine years of estimated pressures are displayed in the figure. The jagged lines on the plot are due to the fact that monthly average rates have been imposed. Again the oscillations in pore pressure due to production fluctuations are quite small, less than about is ± 0.12 bar. At greater distances from the well the values of pressure drawdown are even smaller (± 0.025 bar at 1 km from the well).

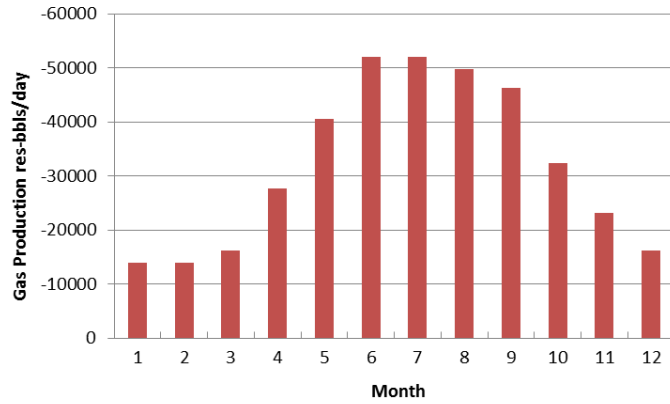


Figure 5. Imposed production rates for the analysis of seasonal production variations. This represents the variation reported in Figure 6.

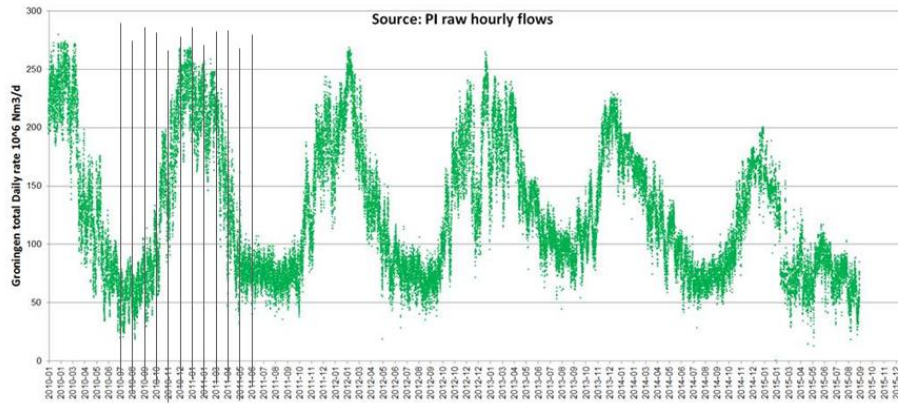


Figure 6. Groningen production data, reflecting the magnitude of seasonal production swings. Vertical black lines are the points in time used to determine the imposed rate in Figure 5.

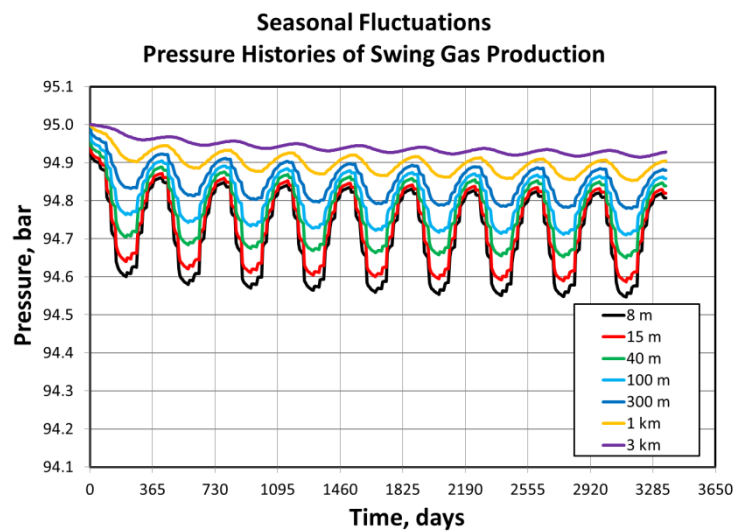


Figure 7. Pressure histories at various distances from a well reflecting seasonal production variations for base case permeability of 150 mD

The cases presented so far have been artificial production histories for wells in an infinite acting reservoir. While large, the Groningen field does not act as an infinite reservoir. Pore pressures decrease with time due to the large amount of production so in addition to the pressure variations due to daily or seasonal fluctuations in production, there is a long term steady state decrease in pore pressure superimposed on this trend. The long term average depletion rate was approximately 3 bar/year and the pore pressure history can be approximated by superimposing this trend on the fluctuation calculations like those shown in Figure 3 and Figure 7.

The 't-Zandt-2 well was chosen as a representative well and seven months of daily production data from this well were used to examine what a realistic pore pressure history might look like. The daily production from the first half of 2009 is shown in Figure 8a. The transition from high to low production rates in April of 2009 is due to the seasonal swing in production as less gas is produced as spring arrives. Figure 8b illustrates the pore pressure history around a 't-Zandt-2 well in an infinite reservoir while Figure 8c is the same pressure history with a 3 bar/year decrease superimposed to reflect the long term depletion of the Groningen field. In the absence of the long term trend, the pore pressure history is not monotonically decreasing. Even 1 km away from the wellbore the pore pressure increases and decreases. However, once long-term depletion is accounted for (Figure 8c) the pressure histories at roughly 150 m from the wellbore become almost exclusively monotonically decreasing. Therefore, most of the field would not be following a cyclic stress path, but rather a path of increasing stress at a non-constant rate.

Most of the production wells in the Groningen field occur in clusters where the wellbores are ~100-200 m apart from each other. An average cluster may have ~ 5 wells operating. In order to determine the upper bound effect of production from a cluster, Figure 8d and e illustrate the pore pressure history around a wellbore with 5 times the production of the 't-Zandt-2 well. This is an upper bound to the behavior because in this example all the production is coming from one well location while in reality the wells are separated by a finite distance. Therefore the 10 m and the 40 m distance lines are not achievable because production is not that localized. The 500 m and 1 km pore pressure histories are more in line with the actual pore pressure histories. The 1 km line is monotonically decreasing but the 500 m distance pore pressure history has some slight increases in the predominantly decreasing trend. This implies that there are some portions of the field that do not exhibit a monotonic increase in fault loading, but much of the reservoir follows a roughly monotonic path.

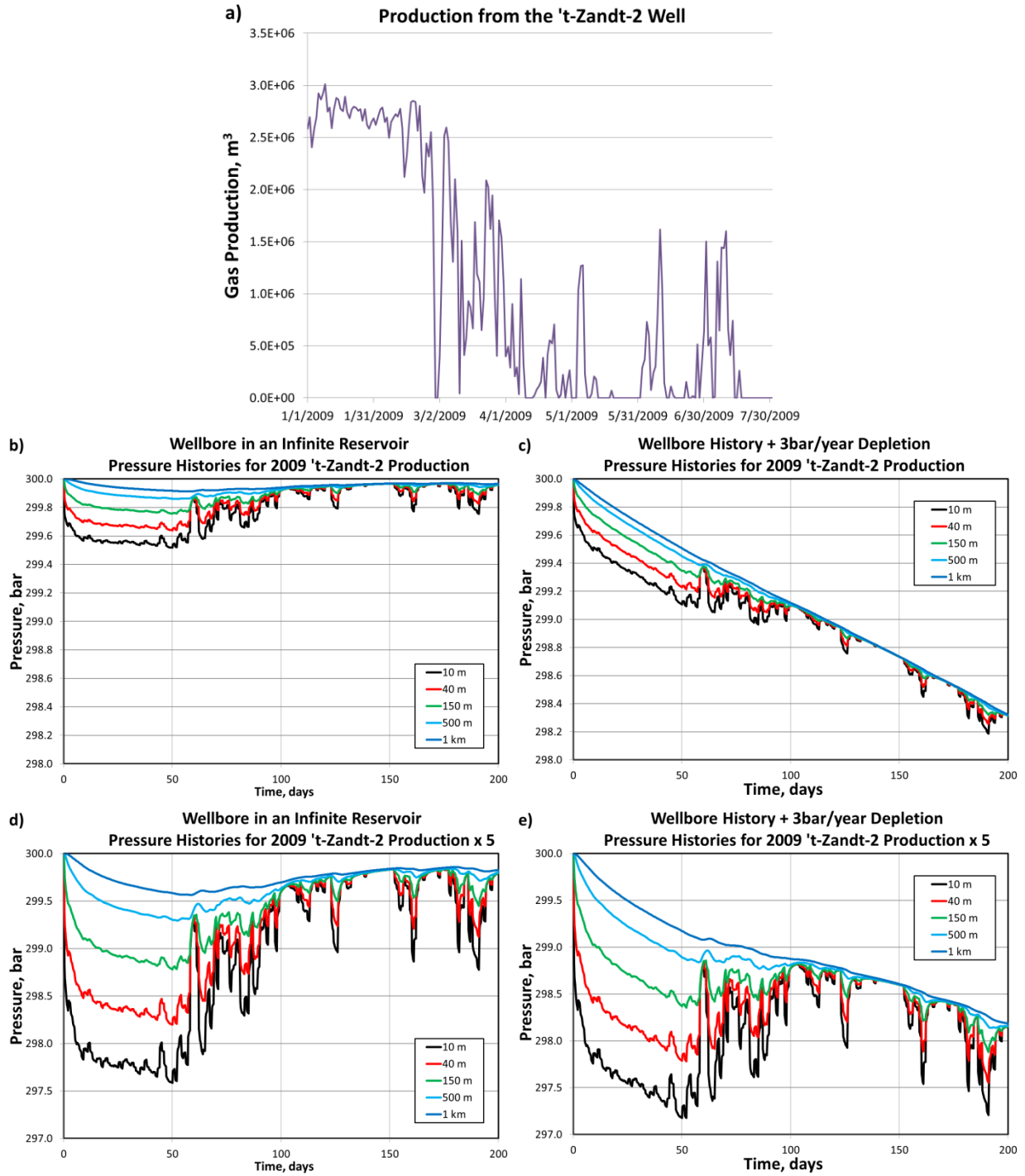


Figure 8. Pressure histories at various distances from a well based on historical production data. (a) Production history of the 't-Zandt 2 well, (b) Pressure history if the well was in an infinite reservoir (c) Pressure history when 3 bar/year depletion is superposed on the histories shown in (b), (d) Pressure history for a well with five times the production, meant to represent a production cluster at long distances, in an infinite reservoir (e) Pressure history when 3 bar/year depletion is superposed on the histories shown in (d)

2.3 Summary and Conclusions

The average pore pressure in the field is decreasing but localized areas in the vicinity of wellbores (within ~200 m) may experience pore pressure increases and decreases due to seasonal and daily fluctuations in production. The magnitudes of these fluctuations in pore pressure are very small ($\sim\pm 0.1$ bar) in comparison to the general level of reservoir depletion at Groningen, which is over 200 bar. The limited spatial extent and small magnitude of the effect suggests that the effect of fluctuations in production should be small and the aggregate seismic hazard should be mostly dependent on the cumulative production/depletion.

However, even small differences in how the faults are loaded (i.e., stress loading history) could have an effect on the resulting seismicity. In the case of monotonically decreasing pore pressures the faults in the reservoir are slowly being brought closer and closer to failure potentially at either a constant or non-constant (in the case of fluctuations in production) rate. If pore pressure increases occur, the faults are brought towards failure and then away from failure during every production cycle. This difference in the stress path could have implications for the effect on seismicity.

3.0 Geomechanical Modeling of Earthquake Cycles

A new geomechanical model has been developed to simulate earthquake catalogs by implementing a rate-and-state frictional description of the fault. This formulation is well suited to address the issue of production fluctuations because the “state” portion of the formulation makes the result dependent on the sliding history of the fault and could allow for differences in behavior based on the production (or stress) history. Section 3.1 describes rate-and-state friction, and how it differs from traditional Coulomb friction. The following sections describe the results of two implementations of rate-and-state friction. A simplified model that addresses earthquake activity, but not magnitude, is presented in section 3.2. A complete rate-and-state model that solves for event frequency as well as event magnitude is presented in section 3.3. Despite the inclusion of additional physics, both the complete model and the simplified model conclude that the character of the seismicity is not dependent on the stress history.

3.1 Introduction to Rate and State Friction

Fault sliding behavior is often described using Coulomb frictional sliding. In this framework a fault begins to slide once the shear stress, τ , on a fault exceeds the failure strength of the fault, τ_{peak} . The strength of the fault is the product of the effective normal stress, $\bar{\sigma}$, and the coefficient of friction, μ .

$$\tau = \mu \bar{\sigma}$$

A notable feature of this model is that the coefficient of friction is a constant and unchanged by the amount of slip, the slip velocity, the stress history or any other parameter. Depending on the fluctuations, the fault will experience a different stressing history on the way to failure, but this history will have no effect on the failure with Coulomb frictional sliding. Since there is no rate or history dependence captured by this law, Coulomb friction is poorly suited to address questions about the effect of fluctuations in production.

In addition to not being able to account for variable stress history, Coulomb friction is also unable to explain several observations of real rock behavior that may play a large role in controlling fault failure. Namely, Coulomb friction cannot account for a coefficient of friction that is sliding rate dependent and time dependent. Here the coefficient of friction is defined simply as the ratio of the shear to effective normal stresses required to maintain motion on a slipping surface.

It has been observed that friction changes with sliding rate. Figure 9a illustrates the velocity dependence of the coefficient of friction during a velocity stepping experiment in the lab. In this type of experiment the simulated fault surface is first slid at a low velocity and then at a higher (10x faster) velocity. At the initial sliding velocity, the coefficient of friction of this sample is 0.545 and then at the faster velocity, the steady state friction value is 0.541. There is an instantaneous increase in friction value following the step to a higher velocity (strengthening) but this effect is short lived as the simulated fault surface ultimately becomes weaker with increased velocity. This behavior is called velocity weakening. For some experimental conditions (different pressures, temperatures or materials) velocity-strengthening may also be observed. Whether a fault is velocity weakening or strengthening has implications for how it will behave when it fails. Velocity weakening results in an unstable process that promotes seismogenic behavior: faster slip makes the surface weaker, so slip can occur faster, so the surface gets weaker, and

so on. In contrast velocity-strengthening materials get stronger with faster slip, so these materials respond with aseismic creep rather than with earthquakes. A velocity (or sliding rate) dependence of fault frictional properties has implications for fault response to stress loading so it is important to include this dependence when evaluating the effects of stress history on seismicity.

Laboratory tests have also shown that the frictional properties of surfaces are time dependent. Slide-hold-slide tests involve sliding the simulated fault surface at a constant rate, stopping and holding the sample in stationary contact for a fixed amount of time, and then re-initiating sliding. Figure 9b shows an example of a laboratory slide-hold-slide test where the sample was held for either 100 seconds or 10 seconds. The longer the hold the larger the transient frictional response, indicating a history dependent healing process.

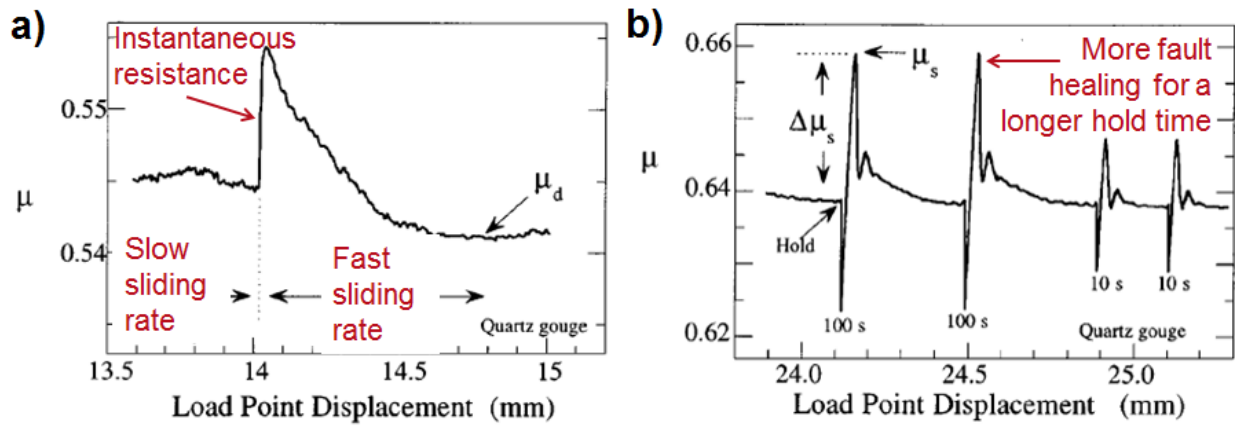


Figure 9. Laboratory tests illustrating the (a) velocity and (b) state (or time) dependence of the frictional properties. Figures modified from Marone, 1998.

Laboratory tests revealed that there are properties of friction that are not captured by Coulomb friction. Friction is not a constant but rather an evolving quantity dependent on velocity, V , and time, captured via the state variable, θ , that describes the sliding history (or state) of the surface.

$$\tau = \mu(V, \theta)\bar{\sigma}$$

One way to interpret the state variable is that it is the duration of a contact. Upon seismic slip the state variable resets and then grows while the fault is stationary. Consequently, there is a competition between the fault loading and the healing process that determines the strength of the fault and this strength (and susceptibility to slip) changes throughout the seismic cycle.

In the rate-and-state framework, the coefficient of friction evolves according to the following equation

$$\mu = \mu_0 + a \log_{10} \left(\frac{V}{V_0} \right) + b \log_{10} \left(\frac{V_0 \theta}{L_f} \right)$$

Where μ_0 is the reference friction value, V_0 is the reference sliding velocity, a , is the magnitude of the instantaneous response, b is the magnitude of the evolving friction response, and L_f is the length scale

over which friction evolves to the new quantity. The surface is velocity-weakening if $a - b < 0$ and velocity strengthening if $a - b > 0$.

The state parameter evolution is governed by its own ordinary differential equation (ODE) so the state evolves in time. The evolution accounts for breaking of contact points on the fault (asperities) and fault healing/re-strengthening in between earthquakes. The state is most commonly assumed to evolve based on one of the following laws:

$$\dot{\theta} = 1 - \frac{\theta V}{L_f} - \alpha \frac{a\theta}{b\bar{\sigma}} \dot{\sigma}$$

$$\dot{\theta} = -\frac{\theta V}{L_f} \ln\left(\frac{\theta V}{L_f}\right)$$

The first law is the Aging law (Dieterich and Conrad 1984) and frequently the final term with the normal stress dependence is not included by setting the coefficient, α , to zero. With the aging law the fault heals while in stationary contact and there is a steady state increase in strength with time. The second law is called the Slip law (Ruina 1983) and the state can only evolve during sliding. The fault is relatively weak during the bulk of the interseismic time and only starts to heal as the fault gets closer to failure. The differences between these evolution laws have implications for how faults governed by these laws will respond to small local stress perturbations.

It has been observed that earthquakes are subject to dynamic triggering, where stress waves from teleseismic events result in very small local stress perturbations (~ 0.01 psi). Despite their size, these stress perturbations are sufficient to initiate local earthquake events. Delayed dynamic triggering has also been observed where triggered earthquakes do not occur during the passing of the teleseismic waves, but rather occur sometime later (e.g. Brodsky and van der Elst, 2014). In an attempt to understand this phenomenon, van der Elst and Savage (2015) conducted laboratory experiments on a variety of simulated fault surfaces. The samples were subjected to oscillatory stress perturbations in which the stress did not reach the Coulomb failure limit (these oscillations are analogous to the stress perturbations felt by faults due to changes in production). Even though Coulomb failure was not reached, instantaneous triggering of a stick-slip event occurred as well as delayed triggering of the next stick-slip event. In the case of instantaneous or delayed triggering the earthquake occurred earlier than expected given the periodic stick-slip nature of the sample. The numerical investigations in van der Elst and Savage (2015) conclude that the rate-and-state framework is able to explain many of the characteristics observed in the lab but neither state evolution law is able to explain all of the observations. Consequently both laws are examined here.

There are several timescales that control the behavior of the rate-and-state friction equations. One of these timescales is the timescale for nucleation, t_a , which was highlighted in Dieterich, 1992 and Dieterich 1994 and is on the order of 1 year. Given this long duration, monthly or higher frequency fluctuations in stress history were thought to be unable to alter the behavior, however, laboratory tests and numerical studies of higher frequency oscillations have shown this assumption to be invalid (van der Elst and Savage,

2015). This study will examine fluctuations that range from weekly to seasonal in duration and the rate-and-state equations should be able to capture the effects of these perturbations.

The characteristics of the rate-and-state friction formulation described above make it well suited to address the issue of production fluctuations. Critically, the “state” portion of this formulation makes the result dependent on the sliding history of the fault. This important feature not only captures the real behavior of rocks, but also may allow for differences in production schedule (constant vs. non-constant stressing rate) to affect the characteristics of the induced earthquakes. This separates rate-and-state friction from Coulomb friction as a helpful tool to apply to production fluctuations.

3.2 Earthquake Activity Rate Models

The simplest application of rate-and-state friction is to evaluate changes in the earthquake activity rate as a function of changes made to the shear stressing rate (Dieterich, 1994). The model described below follows this methodology.

3.2.1 Activity Rate Model Background

A background stressing rate (tectonic or anthropogenic) will produce earthquakes at a certain rate, so a change in the stressing rate should change the rate of earthquake occurrence. The magnitude of the earthquake rate change depends on the background stressing rate, $\dot{\tau}$, the normal stress, σ , and the rate-and-state friction parameter, a .

The initial definition of the state in the model domain is critical to any model that implements a state dependence. In a complete model that implements rate-and-state friction, every point in space is a potential earthquake nucleation location and the state variable is defined at each point. Following the methodology used in Dieterich (1994), a bulk representation of the initial state can be derived based on the following assumption: between earthquakes, slip velocities along faults can be non-zero (but small), because faults are observed to creep between earthquakes. Therefore, a distribution in the initial fault slip speeds can be used to develop a bulk representation of initial “state” for all the potential nucleation points. An increase in stressing rate will result in an instantaneous response at each point. For some locations this will result in failure (earthquake) but many of the potential nucleation locations will not fail.

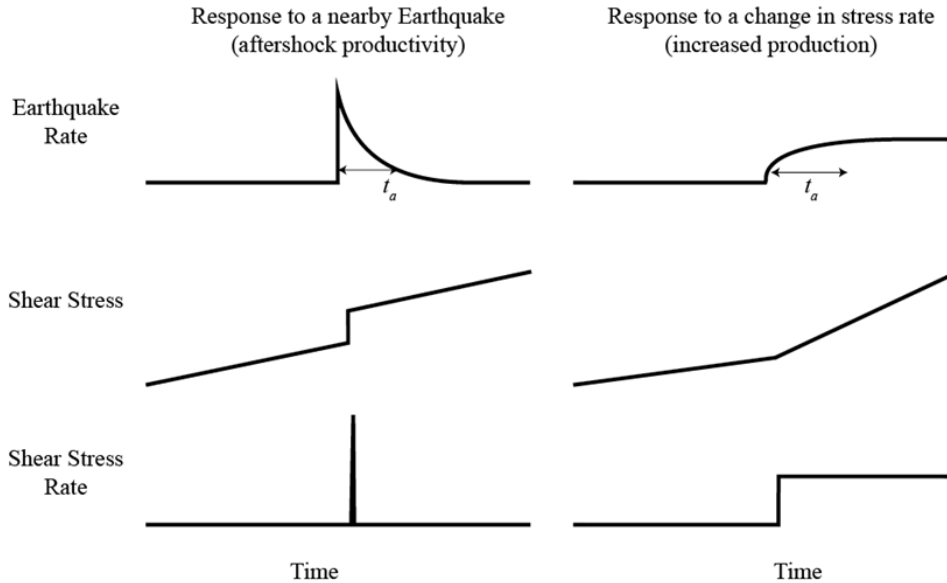


Figure 10: The model from Dieterich, JGR 1994, reproduces observations of aftershock activity (sharp increase followed by a decay back to background earthquake rate). It also characterizes how earthquake rate will adjust to changes in background stressing rate

An assumption made in Dieterich (1994) is that a given background stressing rate (tectonic or anthropogenic) produces earthquakes at a certain rate. Therefore changes in the background stressing rate should translate directly into changes in the rate of earthquake occurrence. The magnitude of the change in earthquake rate will depend on three things: the background stressing rate, $\dot{\tau}$, the normal stress, σ , and the rate-and-state friction parameter, a . This type of model is able to reproduce two types of fault behavior observed in nature. The first is the pattern of aftershock activity after large events (Figure 10). The occurrence of a nearby earthquake is treated as a jump in stress level felt by nearby faults. The surrounding area responds with higher earthquake activity and this gradually settles back to the background activity rate. The second phenomenon this model captures is that a change in the background shear stress rate results in a permanent change to the steady state earthquake rate. Similar to the aftershock case, the adjustment to the new rate takes place over some time scale. The time-scale of this decay/adjustment, t_a , is also known as the nucleation time scale and it depends on the rate-and-state and stress parameters prescribed.

$$t_a = \frac{a\sigma}{\dot{\tau}}$$

3.2.2 Activity Rate Model Parameters

Several key parameters must be chosen to initialize the model. Critically, in order to model changes to the earthquake rate the background earthquake rate must be identified. To obtain a background earthquake rate the year-to-date catalog is examined. In the Groningen field, 25 EQ/year is a representative rate for earthquakes larger than M 1.5, over the past 5 years. If all earthquakes observed are considered, 90 EQ/year is a representative rate.

As described above this model also requires the selection of the background stressing rate, the normal stress, and the rate-and-state friction parameter. A background shear stressing rate of 0.25 MPa/year is assumed based on the increase of shear stress on faults in a static geomechanics model due to production (Lele et al., 2016) but a shear stressing rate of 1.0 MPa/year is also considered. A constant effective normal stress of 20 MPa is assumed. A range in the rate-and-state frictional parameter “a” is examined based on values observed in laboratory testing (see Additionally, if different depletion states are reached at the end of the model calculation, then there may be a large effect on the total number of earthquakes. Therefore the same depletion state must be reached at the end of the model calculation to determine if fluctuations in production are responsible for a change in earthquake occurrence. The final depletion state should be the same whether the field undergoes depletion through constant or variable depletion rates. By imposing a sinusoid variation of the specified amplitude ($\pm 40\%$) it is ensured that the same final stress state is reached after 1 year regardless of the nature of the depletion rate.

Table 2 for a summary of parameters).

Finally, the size and periodicity of the change in the shear stressing rate must be identified. The effect of production fluctuations on the year or day time scale are estimated from the production data and the swing in the month-to-month dissipated energy in the static geomechanics model (Lele et al., 2016). For the seasonal variation (year time scale), a fluctuation of $\pm 40\%$ is assumed. For the daily variation, a fluctuation of $\pm 10\%$ is used based on the data in Figure 4. The results of section 2 show that this 10% oscillation is an upper bound to the perturbation based on the calculated stress perturbation around the wellbore due to daily rate fluctuations.

Additionally, if different depletion states are reached at the end of the model calculation, then there may be a large effect on the total number of earthquakes. Therefore the same depletion state must be reached at the end of the model calculation to determine if fluctuations in production are responsible for a change in earthquake occurrence. The final depletion state should be the same whether the field undergoes depletion through constant or variable depletion rates. By imposing a sinusoid variation of the specified amplitude ($\pm 40\%$) it is ensured that the same final stress state is reached after 1 year regardless of the nature of the depletion rate.

Table 2: Parameters used for in the Dietrich earthquake rate model

Parameter	Variable	Value	Notes
Background earthquake rate	r	25 EQ/yr 90 EQ/yr	Used for $M \geq 1.5$ Used for $M \geq 0.5$
Background shear stressing rate	$\dot{\tau}$	0.25-1.0 MPa/yr	
Effective normal stress	σ	20 MPa	
Rate-and-state parameter	a	.005-0.01	
Seasonal stress rate fluctuation		40%	
Daily stress rate fluctuation		10%	

3.2.3 Activity Rate Results

The effects of both seasonal and daily production fluctuations have been evaluated. To examine the effect of seasonal (1 year time scale) production fluctuations a model with a constant stressing rate is compared to a model with a constant plus a sinusoidal stressing rate for 8 years and then the constant background rate is assumed for two additional years. A comparison between these two stress rate histories is shown in Figure 11. The black line is the constant shear stress rate and the red, blue and green lines represent the spread in model results based on a range on input parameters (red line is the default model parameters). Notably, the response of the earthquake rate is out of phase with the imposed sinusoidal oscillation of shear stressing rate (compare Figure 11 a and b). This delay in model response is due to the parameter, t_a , which varies for the three cases examined here due to the parameter assumptions outlined in Table 2.

The default model parameters described in the figure caption for Figure 11 result in a variability in earthquake rate of ± 5 earthquakes/year (red curve in Figure 11b). However, this is the instantaneous earthquake rate not the cumulative number of earthquakes over a year. The cumulative number of events is the integral of the data shown in Figure 11b. Figure 11c shows the difference between the cumulative number of events for the three fluctuating scenarios under consideration and the constant stressing rate scenario. From Figure 11c it is clear that the effect on the cumulative number of observed earthquakes is small at any given point in time.

The amplitude of the swing in Figure 11c (± 0.5 -1.5 earthquakes) reflects the expected swing in the number of earthquakes observed throughout the year. If 25 events occur per year, during any given year you should expect to be between 0.5-1.5 earthquakes ahead or behind of what would be observed for the constant production scenario. This small difference is unlikely to be an observable signature in given year. In contrast, if the background rate is 90 earthquakes/year, the signature is ± 13 earthquakes and this becomes an observable signature (Figure 12). As discussed in the following section, the predicted small effect on the timing of events throughout the year when 25 events are expected may be why it is difficult to say with certainty that there is a seasonality to the $M \geq 1.5$ events but there is a clear signature if all of the smaller events are included (Figure 12).

The swing in the number of events during the year is not the same as a change in the total number of events. At the end of each model run, after two years at a constant shear stressing rate, the difference between the constant and fluctuating scenarios is negligible. This means that regardless of the stressing history, the same total number of events occur in this numerical model. Notably, the result does not oscillate around zero in Figure 11c and Figure 13c. This is because when the sinusoid is imposed, the cumulative shear stress for the fluctuating forcing is always greater than or equal to the constant scenario. By phase shifting the imposed sinusoid the results can be made to oscillate around zero but this modification does not alter the conclusions.

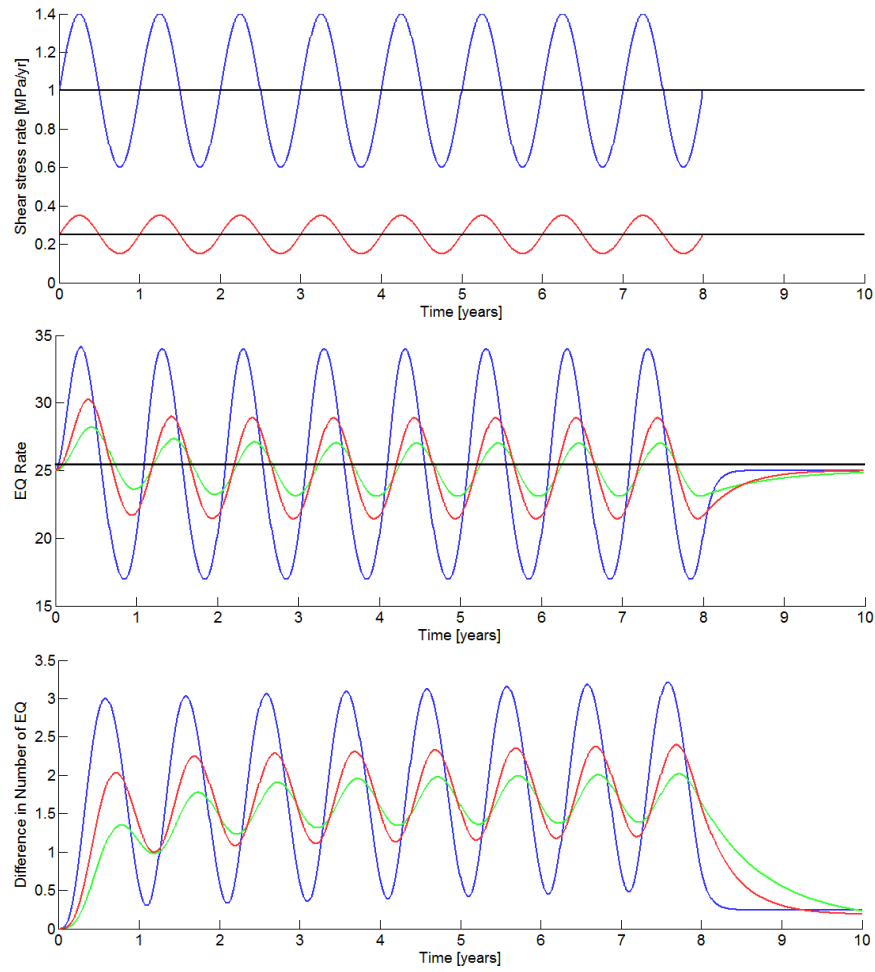


Figure 11: Comparison of the seismicity rates for constant stressing rate (black line) and scenario seasonal production variations. (Black line – constant stressing rate; red line (default parameters) - 25 events/year, 0.25 MPa/year, $a = 0.005$, $t_a=0.4$ year; green line - 25 events/year, 0.25 MPa/year, $a = 0.01$, $t_a=0.8$ year; blue line - 25 events/year, 1.0 MPa/year, $a = 0.005$, $t_a=0.1$ year) (a) Shear stressing rates imposed. Green and red lines are plotted on top of one another. (b) Variation in earthquake rate throughout the year based on the input parameters. (c) Difference between total number of observed earthquakes for scenario between the variable and constant stressing rates. Lines do not fluctuate around a value of zero because the total cumulative shear stress for the variable scenario is always greater than or equal to the constant scenario.

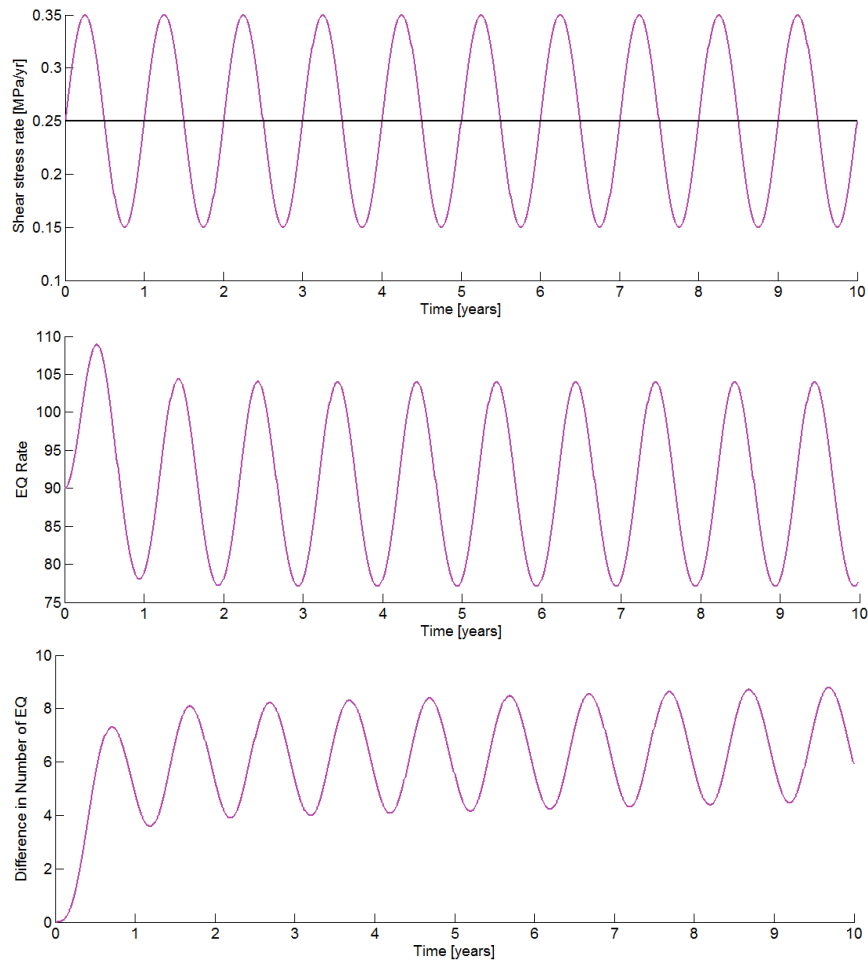


Figure 12: Same as Figure 11 but for a larger background activity rate (90 events/year, 0.25 MPa/year, $a = 0.005$, $t_a = 0.4$ year)

This model can also be used to examine the changes in the number of earthquakes due to daily fluctuations in production. Based on the results of section 2, the assumed fluctuation of $\pm 10\%$ is only valid very close to the wellbore (< 25 ft) so the bulk of the field will feel a much smaller variation in stressing rate. Consequently, a perturbation of this magnitude represents an upper bound on the expected stress perturbation in most of the field. However the potential impact of this large stress perturbation on earthquake rate is limited by the time scale for adjustment, t_a , used in this model. Due to the choice of parameters outlined in Table 2 the time scale for adjustment is on the order of 0.1-1 year, which is much longer than 1 day. Consequently the system is largely unable to respond to an increase in stressing rate before stressing rate begins to decrease. The impact of the combination of these factors on the earthquake rate is shown in Figure 13. The blue and green lines are for the seasonal and seasonal + daily fluctuation cases respectively. There is no discernable difference between the earthquake rate when daily fluctuations are considered (blue and green lines plot on top of one another in Figure 13b and c), even for the exaggerated case examined here.

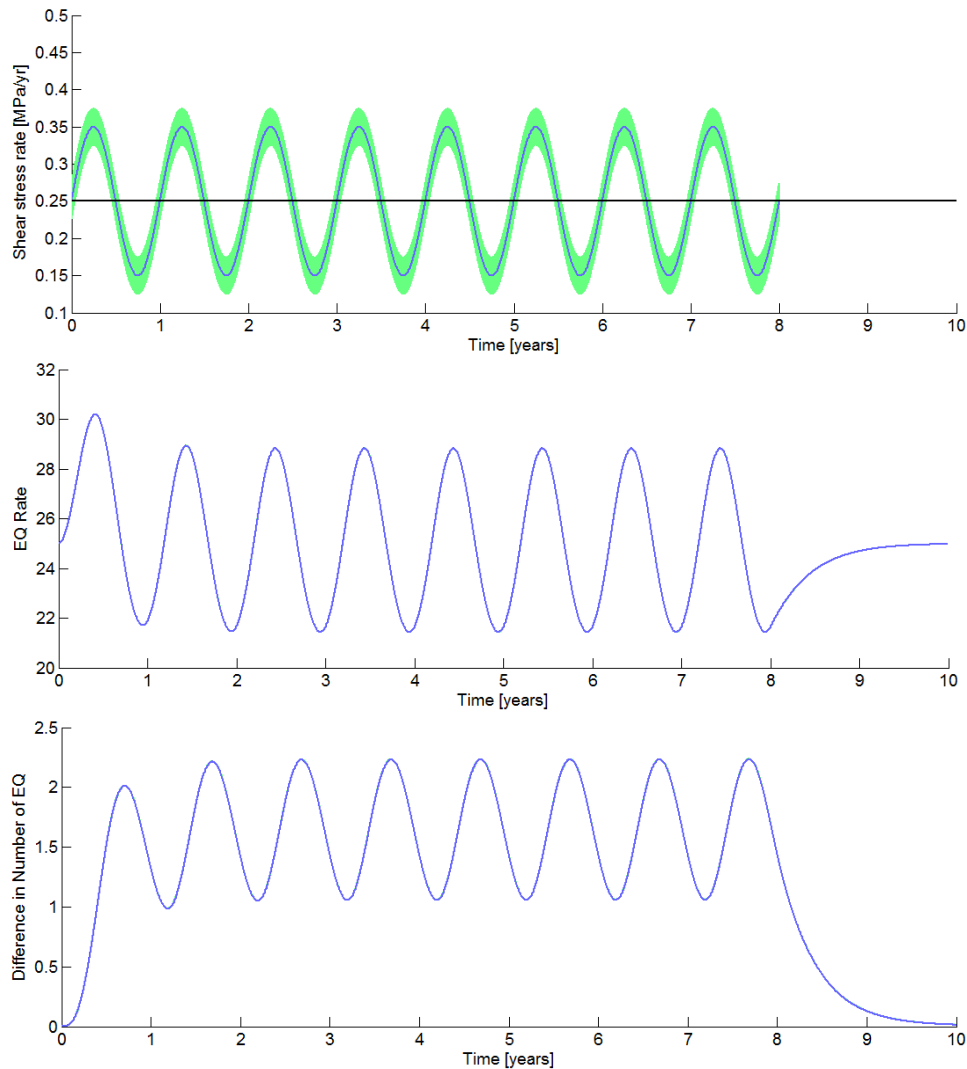


Figure 13: Same as Figure 11 but both seasonal (blue) and seasonal + daily (green) fluctuations in stressing rate are considered. Where no green line is visible the blue and green lines overly one another. (Black line – constant stressing rate) (25 events/year, 0.25 MPa/year, $\alpha = 0.005$, $t_a = 0.4$ year)

This analysis suggests that the total number of earthquakes should not change due to variable production rates for both daily and seasonal variations in production. Consequently the aggregate seismic hazard associated with variable production is not expected to increase above what would be expected for a constant production rate.

3.2.4 Detection of Earthquake Seasonality with Simulated Earthquake Catalogs

The simulated earthquake Poisson activity rate variation throughout the year is quantified in Figure 11b and Figure 13b. The effect of this variation in rate on potential observed events can be examined using a non-stationary Poisson process model. When sampling from a Poisson process with time-varying rate, the resulting earthquake catalogs may or may not reflect the underlying time variance depending on the magnitude of the rate variation and number of events sampled. When more events are sampled, the

aggregate statistics better reflect the time-varying distribution (a law of large numbers effect) thereby enabling the detection of the underlying time-varying earthquake rate. In contrast when fewer events are sampled, the observations may be inadequate in aggregate to infer an underlying trend in activity rate even if the trend was strongly cyclical.

Observations show that the seasonal variation in activity is observed when all earthquakes are included but it is difficult to detect when only $M > 1.5$ events are included (Figure 11). The difference in the number of earthquakes in these catalogs suggests that the signal should be more apparent if more earthquakes are considered. In the case of the ~ 250 earthquakes larger than $M 1.5$, some catalog realizations reflect the underlying sinusoidal variation in earthquake rate and some do not. Once the total number of earthquakes observed is increased to ~ 900 in total, most of the simulated catalogs reflect the underlying variation while a few do not. Consequently, this model indicates that very high rates of seismicity would be needed to conclusively reflect the signature of an imposed sinusoidal variation in stressing rate.

3.2.5 Activity Rate Conclusions

The earthquake activity rate model does not suggest that there will be a difference in the aggregate hazard due to fluctuating versus constant production. This is based on a comparison of seasonal and daily fluctuations in shear stressing rate to a constant shear stressing rate. For all the scenarios the same number of earthquakes was predicted to occur by the end of a simulated year. However, this model is based on a simplified implementation of the rate-and-state equations that would not be able to explain the laboratory observations of van der Elst and Savage (2015), discussed in section 3.1. Additionally, this model does not include information about earthquake magnitude. The simplifications made in this section may be neglecting a significant portion of the underlying physics so a complete implementation of rate-and-state friction is examined in the following section.

3.3 Earthquake Cycle Models

Earthquake cycle models are used to simulate many earthquake events over a period of time and rate-and-state friction is generally applied to govern the frictional behavior of the simulated fault (e.g. Lapusta et al., (2000), Liu and Rice (2007), Kaneko et al., (2011)). These models capture the shear stress evolution during both seismic and interseismic times with the use of variable time-stepping algorithms. The models are discretized over space so portions of the fault can rupture independently (resulting in variable magnitudes) and the time intervals between events depend on the initial and boundary conditions. As a result, these models are able to generate simulated earthquake catalogs with variable characteristics. Since these models produce earthquake catalogs and have history dependence (via the state variable), they are well suited to examine if fluctuations in production alter the character of the seismicity.

These models have primarily been used to study tectonic events but recently they have also been applied to the problem of induced seismicity. Dieterich et al., (2015) examined a simulated earthquake catalog resulting from wastewater injection near a fault. An initially heterogeneous shear stress distribution was applied to a 2D planar fault and then pore pressures were locally increased to simulate nearby injection, resulting in the migration of a pressure front across the fault. As the pressure plume grew, earthquakes were triggered over an expanding area of the fault. Eventually, injection was stopped but a substantial number of simulated earthquakes continued to occur as the pressure plume migrated due to pressure

diffusion. Recently, the same model was applied to examine the effect of cyclic injection near a fault (Kroll, 2016). Two scenarios were examined: 1) constant injection at a specified rate, and 2) alternating years of injection at twice the rate and no injection. These two scenarios resulted in different simulated earthquake catalogs. In the single example presented, the periodic injection scenario resulted in fewer events but a larger moment release, indicating more, larger events with periodic injection. To determine if a change in the hazard can be anticipated at Groningen due to variable production, this study looks for changes in the character of the simulated seismicity such as those highlighted by the example of Kroll (2016).

To determine if variable production is driving change in the character of seismicity this study will subject a fault with a heterogeneous shear stress distribution to three distinct stressing histories. The three scenarios represent three ways of reaching the same total production throughout the year: 1) constant production rate, 2) seasonal swing in production, representing more winter production, and 3) weekly variability of one week on, 3 weeks off. The initial shear stress distribution will determine roughly where and when earthquakes occur while the variable stress histories will alter the state variable evolution for the three scenarios examined. The resulting differences in spatial distribution of the state variable at the time of earthquake nucleation should result in different earthquake catalogs for the three scenarios. Since the catalog is strongly influenced by the initial stress conditions, the resultant catalog from any given set of initial conditions should not be evaluated in isolation. The results of many initially random initial conditions should be viewed in aggregate to determine if there is a statistically significant difference between the catalogs generated for the three stress histories.

The following sections describe how the earthquake cycle model works, the parameter space examined, and the effect of stress history on the earthquake catalog.

3.3.1 Earthquake Cycle Model Setup

3.3.1.1 *Model Geometry*

The ideal fault geometry would be a 2D rough fault in a 3D half space. Models of this sort are achievable but the computational demands result in prohibitively long model runtimes given the number of realizations required for statistical significance. Consequently, only planar faults are examined with discretization in either the strike or dip dimensions. This geometry is referred to as 1.5D since the second dimension of the fault is not fully represented, but the fault still exists in a 3D half space.

A planar fault geometry is assumed at a fault dip that is representative of faults in the Groningen field. Seismically observed fault dips range from 60-90° so fault dips of 70° and 75° are used in this study. Real faults are not perfectly planar surfaces so there is a large amount of heterogeneity in the spatial distribution of stress. Rather than accounting for this using a spatially variable strike and dip, the model is initialized with a heterogeneous shear stress distribution (discussed in more detail later) so that the effect of fault roughness is captured.

The planar fault is discretized into a number of cells in the strike, N_s , and dip, N_d , dimensions. A 2D fault representation (3D model geometry) would have N_s and $N_d > 1$, however, as mentioned above, this requires a prohibitive amount of model run time so 1.5D fault representations are examined instead.

Figure 14 illustrates the setup of the two 1.5D model geometries examined. The model in Figure 14a is used to examine the along strike earthquake geometry ($N_d = 1$ and $N_s > 1$) and the geometry shown in Figure 14b is used to examine the effect of downdip variations in shear stressing rates due to depletion induced stress changes ($N_s = 1$ and $N_d > 1$).

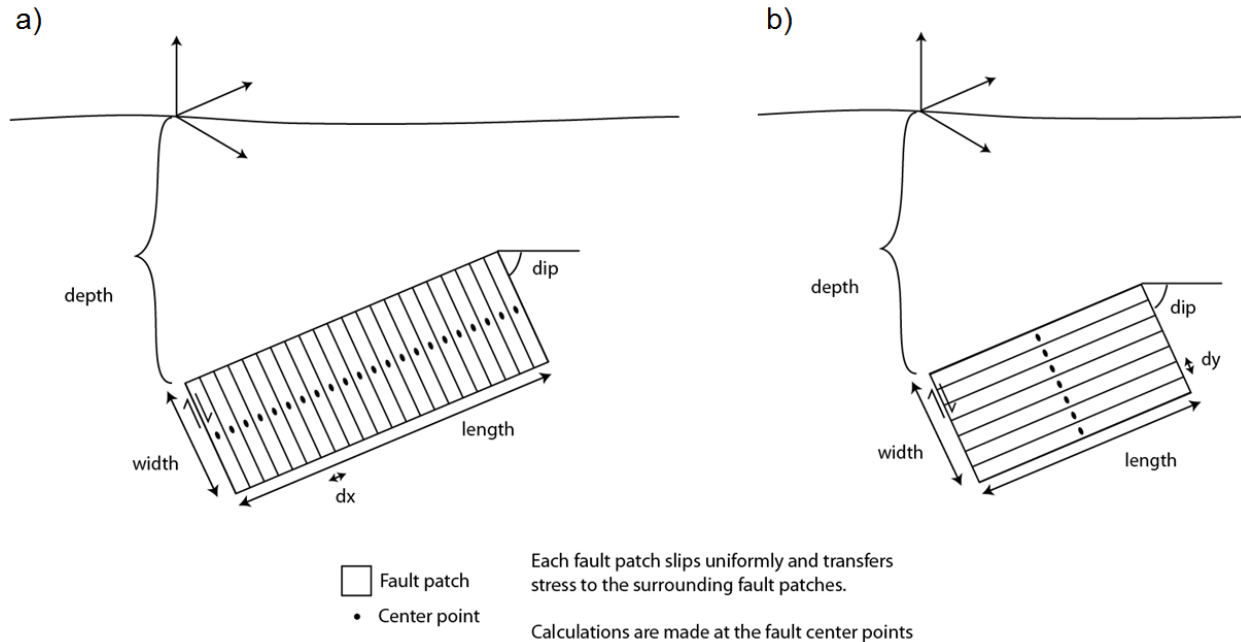


Figure 14. Model geometries used to examine effect of production fluctuations. (a) Strike model and (b) dip model.

3.3.1.2 Governing Equations

The fault is embedded in an elastic half space (Shear modulus, $G = 12$ GPa and Poisson's ratio, $\nu = 0.20$) so the solution of Okada (1992) is used to calculate the quasi-static stress change due to uniform slip over each rectangular fault patch. A stiffness matrix, k , is generated that captures the shear stress change at each fault patch center point due to slip on every fault patch. It is assumed that all fault motion is dip-slip motion so only normal and shear stress changes in the dip-slip direction are calculated. As a consequence of the dip-slip assumption is that as the rupture propagates along strike (as in the model geometry for Figure 14a) it is a mode III propagating crack front. In contrast, a dip propagating rupture (as in the model geometry of Figure 14b) is a mode II propagating crack.

Slip on any fault patch transfers stress to every other fault patch. In a fully dynamic model the stress is transferred to the surrounding fault patches as the stress waves reach the surrounding material. The timing of this stress transfer to other fault patches is determined by the S wave speed, V_s , of the material and the distance between the fault patches. In a true dynamic model this wave propagation is explicitly captured in the off-fault material. The implementation here is a "quasi-dynamic" approximation following the implementation in Rice (1993) in which stress transfer from one fault patch to all other fault patches is instantaneous (i.e. infinite wave speed) but the energy outflow from the slipping patch (as seismic waves) is captured by the addition of a radiative dampening term. This term is proportional to the sliding

velocity, V , so it only becomes important at high slip rates and it assures that a solution continues to exist at high slip velocities, where a quasi-static calculation would result in an instability. When the radiation dampening term is defined as $GV/2V_s$, this term exactly captures the elastodynamic result for how instantaneous changes in shear stress and slip velocity are related to one another. However, Lapusta (2000) showed that the radiation dampening approximation generally results in rupture events with slip velocities 10-100 times slower than the exact, fully dynamic, solution.

As is commonly done, fault patch changes in normal stress due to slip on other fault patches are not included in this analysis for the following reasons. Liu and Rice 2007 included the effect of normal stress changes due to slip in some calculations and found the results to be insignificantly different from those results that ignored changes in normal stress. Additionally, excluding the calculation of normal stress changes decreased the model runtime without a significant effect on the results.

Based on the above considerations, the shear stress on any fault patch, j , at any point in time can be calculated from the following equation

$$\tau_j = \tau_j^0 + \Delta\tau_j^{prod}(t) + \sum_i k_{ij}u_i(t) + \frac{G}{2V_s}V_j$$

Where τ^0 is the initial shear stress distribution, $\Delta\tau^{prod}(t)$ is the shear stress change due to production, u is the amount of slip on all of the fault patches, i , and k_{ij} captures the change in shear stress on patch j due to slip on patch i .

In the rate-and-state framework fault sliding velocity is never truly zero so the fault is always slipping. At higher velocities the shear stress is calculated as the product of the effective normal stress and the coefficient of friction according to the rate-and-state friction equation discussed in section 3.1

$$\tau = \bar{\sigma}\mu = \bar{\sigma}\left(\mu_0 + a \log_{10}\left(\frac{V}{V_0}\right) + b \log_{10}\left(\frac{V_0\theta}{L_f}\right)\right)$$

However, at low sliding velocities a regularized form of this equation must be used (Rice and Ben-Zion, 1996)

$$\tau = \bar{\sigma}\mu = \bar{\sigma}a \operatorname{arcsinh}\left[\frac{V}{2V_0} \exp\left(\frac{\mu_0 + b \ln(V_0\theta/L_f)}{a}\right)\right]$$

By equating the above two equations for the shear stress (calculated as $\bar{\sigma}\mu$) and the above equation for the history dependent shear stress evolution (including the sum over ku), it is possible to derive an equation for the sliding velocity, $V = du/dt$, or dV/dt , dependent on t and θ . This ODE, and the state variable evolution equation for $d\theta/dt$ (section 3.1) are coupled ODE's that can be solved to determine the rate and state evolution of the fault over time.

It is important to ensure proper space discretization for the model parameters chosen in order to ensure accuracy of the calculation. Specifically it is necessary that if one cell is perturbed from part of a uniformly

slipping patch, that perturbation must decay. If perturbations did not decay cells could fail independently of each other and the results would then depend on the spatial discretization. To insure that cells cannot fail independently, the element size, h , must be smaller than the critical cell size, h^* , be larger than. Following Rice (1993) and Lapusta (2000), the cell stiffness helps determine the relevant value for h^*

$$h^* = \frac{2GL_f}{\pi(1-\nu)(b-a)\bar{\sigma}}$$

In the above equation L_f is the characteristic slip distance over which the state variable evolves. By specifying the ratio of $h^*/h = 4, 8, 16 \dots$ and the fault patch size, h , the above equation can be used to determine the value for L_f for a given spatial discretization. In contrast, for implementations where the normal stress changes in time, the initial effective normal stress is used to solve for L_f . This parameter is analogous to the critical slip weakening distance, D_c , frequently used in fully dynamic rupture models.

Table 3. Summary of parameters used in earthquake cycle models

	Strike model	Dip model
Fault dip	75°	70°
Fault depth	2.7 km	2.8 km
Fault width	500 m	275 m
Fault length	10 km	1.5 km
V_0	1e-6 m/s	1e-6 m/s
μ_0	0.6	0.6
G	12 GPa	12 GPa
ν	0.2	0.2
a	0.015	0.015
$a - b$	-0.004, -0.008	-0.004
h^*/h	4, 8, or 16	8
h	5 m	0.1 m
$\bar{\sigma}$	190, 300 bar	150-570 bar
L_f	xx	Xx
τ_{mean}^0	43.5, 100 bar	30-60 bar
τ_{dev}^0	15, 25, 35 bar	40 bar
Reservoir thickness	NA	200 m
Reservoir offset	NA	25, 50, 100, 150, 175 m

3.3.1.3 Model Initial Conditions

It is assumed that there is initial stress heterogeneity on the fault due to both geometric roughness and the cumulative effects of non-uniform stress drops during prior earthquakes. Assuming fault mechanical properties vary relatively smoothly, the initial shear stress distribution must be heterogeneous because earthquakes initiate at a point. If a fault was uniformly stressed the entire fault would start to slip at the same time. At the time of initiation only a small portion of the fault is experiencing shear stresses high enough to fail (the nucleation point) while the neighboring portions of the fault are experiencing lower stresses. Separate from nucleation, it is rarely observed that faults slip in their entirety during an earthquake. This is true even in the absence of large changes in fault geometry that could arrest an

earthquake rupture. This suggests that earthquake propagation can also be arrested by areas of low shear stress because these areas are unable to sustain a rupture.

In the geomechanical model here there is no geometric complexity so rupture propagation can only be stopped by areas of low shear stress. Without low stress barriers to propagation, most of the modeled fault will fail in each event and the resulting earthquake catalog will have a uniform magnitude. Therefore, this model allows for shear stress heterogeneity and captures this heterogeneity with an initial shear stress distribution, τ^0 .

The initial shear stress heterogeneity is assigned following the procedure outlined in Dempsey and Suckale (2016). This methodology assumes that the shear stress on the fault is consistent with a fractal model with a fractal exponent of $n = 0.25$. The value of the exponent determines the degree of spatial coherency (high values are dominated by long wavelength features and therefore have a high degree of spatial coherency). Each model run is initialized by generating a vector of random phase angles, multiplying this with the wave number vector in the wave number domain, and then calculating the inverse Fourier transform to obtain a first pass spatial distribution of shear stress on the fault. Following Dempsey and Suckale (2016), this first pass is then rescaled so that the distribution of shear stress follows a Gumbel distribution with a specified mean, τ_{mean}^0 , and standard deviation, τ_{dev}^0 . Each vector of random phase will generate a different initial shear stress distribution. An example of the initial shear stress distribution is presented in Figure 15 for $\tau_{mean}^0 = 100$ bar and $\tau_{dev}^0 = 25$ bar.

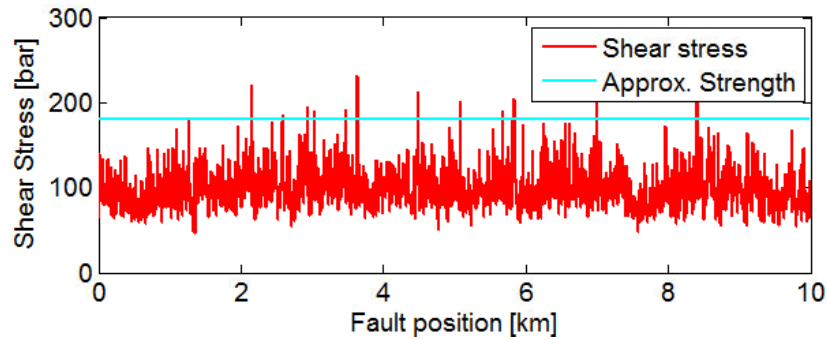


Figure 15. Example of initial shear stress distribution for specified parameters $\tau_{mean}^0 = 100$ bar and $\tau_{dev}^0 = 25$ bar.

At time $t = 0$, the shear stress obeys the law:

$$\tau_0 = \bar{\sigma} \left(\mu_0 + a \log_{10} \left(\frac{V}{V_0} \right) + b \log_{10} \left(\frac{V_0 \theta}{L_f} \right) \right)$$

Many of the parameters in the above equation are constants (a, b, μ_0, V_0 and L_f) so either V or θ must be spatially variable to achieve the initial variation in shear stress. It is reasonable for different points on the fault to have different values for the state variable because they have different sliding histories. Here a constant initial velocity is assumed and then it is possible to solve for the initial, position dependent θ value that satisfies the above equation. Due to the imposed variation and the coupled ODEs, the initially uniform sliding velocity quickly evolves to a spatially variable value in the first few time steps. Since the

velocity quickly adjusts to balance the imposed initial condition, the choice to initialize the model by attributing the variation entirely to the state variable is unlikely to be affecting the results of the model.

3.3.1.4 *Model Boundary Conditions*

Several different methodologies can be employed to drive an earthquake cycle model to failure. The simplest scenario is to hold normal stress constant and increase shear stress. This is the loading scenario that would be most commonly implemented in a tectonic regime. In the case of seismicity induced by oil and gas extraction, or by waste water disposal, there are changes in pore pressure that result in changes in effective normal stress so the assumption of a constant normal stress is not appropriate. However, only one form of the state variable evolution law is sensitive to changes in normal stress. Consequently it is still useful to examine the simple scenario of constant normal stress and increasing shear stress to more fully assess the effect of parameter choices and shear stress history on the resulting earthquake catalogue. Three methodologies for boundary condition implementation are considered. Some methods consider realistic spatial dependence of the change in shear and normal stress and some are simplified to allow for the examination of other parameters.

Methodology A is the simplest stress scenario of a constant normal stress and time dependent shear stress. The effective normal stress is chosen to be 300 bar at every fault patch and an initial heterogeneous shear stress distribution is determined. Production induced changes in shear stress are then specified as a function of time $\Delta\tau_j^{prod}(t)$ and are used to uniformly increase the shear stress on the fault and bring the fault closer to failure. The entire fault is subject to the same increase in shear stress.

While any shear stress history can be implemented, three basic time histories are examined and shown in Figure 16. The base case is that of a linearly increasing shear stress in time, or a constant rate of shear stress increase (blue line in Figure 16). This represents the constant production scenario with no fluctuations in production. The second case is a seasonal swing in production (red line in Figure 16). A sinusoidal oscillation of variable amplitude is superposed onto the constant production rate. Depending on the amplitude of the oscillation, the shear stress can monotonically increase (but at a non-constant rate) as shown in Figure 16b, or with a larger amplitude oscillation, stress can both increase and decrease, which may be more representative of the stress path for faults close to production wells. The third stress history scenario (“week”) examined is meant to represent a more variable production history: 1 week of production, followed by 3 weeks of no production, and repeat. The one week of production is represented by a shear stressing rate with the functional form of half of a sinusoidal wavelength. The rate starts and ends the week at zero and reaches a very high rate in between. The shear stressing rate is zero during the 3 weeks off. Figure 16a illustrates the shear stressing rate and Figure 16b shows the cumulative increase in shear stress (the integral of the lines in Figure 16a). All three stress histories result in the same shear stress state at the end of the year. In the cases shown here the non-constant scenarios always have a shear stress level greater than or equal to the constant scenario. By shifting the phase of the sinusoidal oscillation it is possible to alter this so that the fluctuating scenarios are centered around the constant scenario line (Figure 16c). This alternate scenario was also examined but did not alter the conclusions of the study.

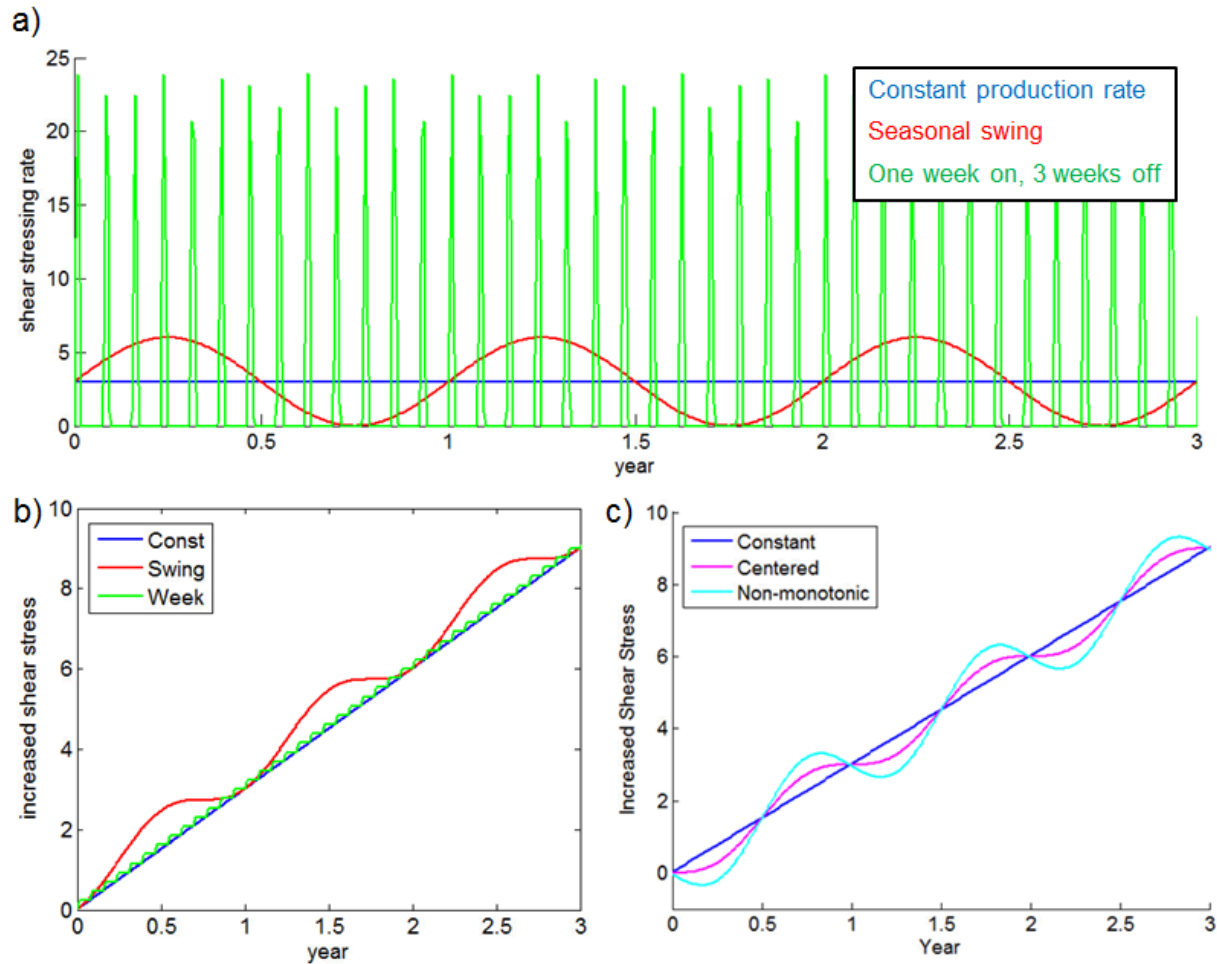


Figure 16. Three stress histories are applied to all model setups to examine the effect of stress history on the earthquake catalog. (a) Shear stress rate applied in methodology A or pore pressure depletion rate applied in methodologies B and C. (b) Cumulative shear stress increase due to production applied in methodology A or pore pressure depletion history applied in methodologies B and C. (c) Alternate scenarios considered in methodology A implementation that include a phase shift from that shown in (b) so that the swing shear stress history alternates between above and below the constant rate and allows for a non-monotonically increasing shear stress history.

Methodology B incorporates both shear and normal stress changes in to the fault stress history. An approximation to the stress path followed by a fault during production can be made with the assumption of uniaxial strain boundary conditions. Under this assumption, as the pore pressure in the reservoir decreases, the total vertical stress stays constant and the total horizontal stress decreases. The result is that both the effective normal stress and shear stress on the fault increase with depletion. Depending on the elastic parameters, the fault can either move towards or away from failure. For example, for a Poisson’s ratio of 0.2, and a fault dip of 70°, the shear to normal stress ratio on the fault decreases with depletion, so the fault moves away from failure. However, this is contrary to the observation that earthquakes have occurred as the reservoir has been depleted and highlights the fact that there are many effects not accounted for under the assumption of uniaxial strain deformation. Uniaxial deformation may be representative of the evolution of reservoir material far away from the fault, but the geometry around

a pre-existing fault (specifically the fault throw) makes this approximation less applicable. The fault geometry can lead to areas of the fault undergoing much larger increases in shear stress. Therefore methodology B uses the uniaxial strain approximation to determine the normal stress increase per increment of pore pressure depletion, and the calculated shear stress increase is multiplied by a factor of two to approximate some of the effects of fault geometry. This results in an increase in the shear to normal stress ratio on the fault and ensures that the fault approaches failure.

The three production histories described previously (constant, seasonal swing and 1week on – 3 weeks off) are also considered for the methodology B implementation. The difference is that rather than specifying shear stressing rates (as in methodology A) the curves shown in Figure 16 are used as depletion rates and the modified uniaxial deformation stress path solution is used to convert depletion rates into shear and normal stress rates. Effective normal stress can change at a non-constant rate, and can increase non-monotonically, allowing for an examination of the effect of including normal stress changes in the state variable evolution equation.

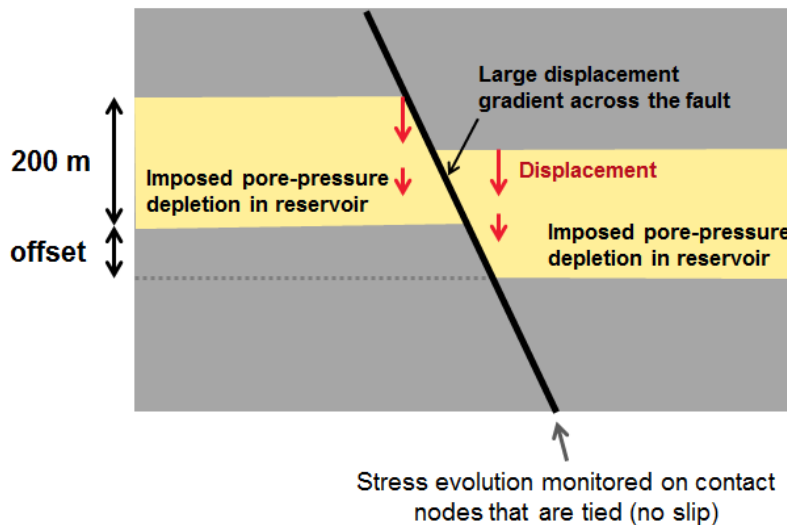


Figure 17. A pre-existing fault offset will result in a position dependent stress history evolution along the dip profile of a fault.

Methodologies A and B both implement uniform stress changes across the entire fault plane and this is well suited for the along strike model geometry (Figure 14a). However, a uniform change in stress is inappropriate for the dip model geometry because the geometrical effects of the pre-existing fault offset result in non-uniform stressing on the fault interface. During depletion the reservoir rock is compacting so the top of the reservoir moves down while the bottom of the reservoir stays relatively stationary (see red arrow indicating displacement in Figure 17). When there is a pre-existing normal fault offset, the top of the reservoir in the hanging wall of the fault is juxtaposed against the bottom of the reservoir in the footwall of the fault. This results in a large displacement gradient across the fault and an increase in shear stress that promotes normal fault motion. The reservoir offset (measured in the vertical direction, not along the fault plane) is therefore a key parameter in determining the stress distribution. For the fault illustrated in Figure 17, the boundaries of the area where reservoir is juxtaposed across the fault have the

largest increases in shear stress. Additionally, the reservoir top and bottom on the footwall and hanging wall respectively will experience a substantial decrease in shear stress. This decrease may provide potential barriers to rupture and could help confine the rupture to the reservoir interval.

To account for the geometrical effects, methodology C implements non-uniform shear and normal stress changes in the dip profile model (Figure 14b). This is done by using the finite element modeling software package ABAQUS to determine the quasi-static stress changes that evolve with production on faults of varying offsets. The changes in shear and normal stress along the fault, per increment of pore pressure depletion, for a range of fault offsets, are shown in Figure 18. Similar to methodology B, the three history scenarios (Figure 16) are implemented as pore pressure histories on the fault, and the shear and normal stress can then evolve non-monotonically and at a non-constant rate depending on the parameters chosen.

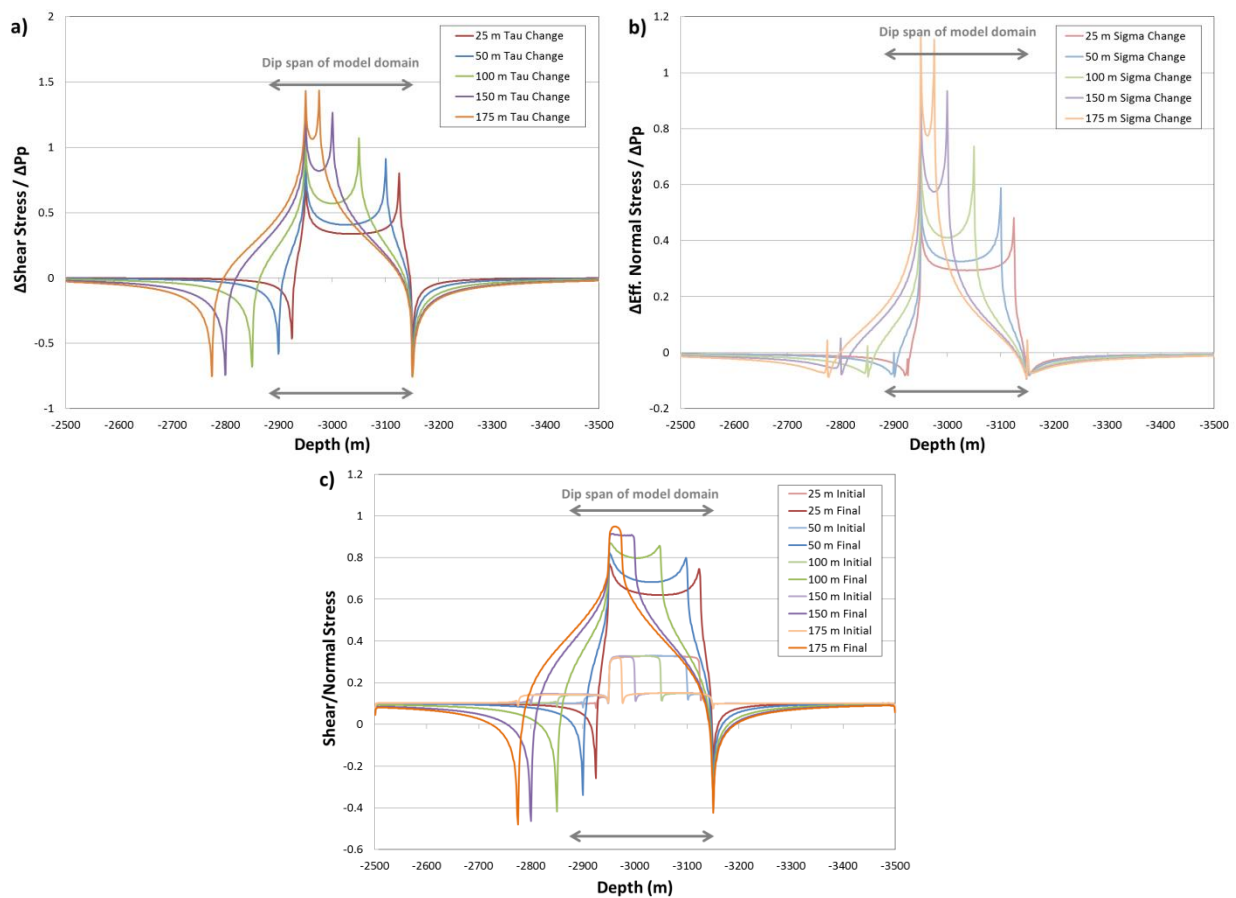


Figure 18. Stress changes on a 70° dipping fault due to homogeneous depletion of the reservoir for a range of initial fault offsets. (a) shear stress change per increment of depletion, (b) normal stress change per increment of depletion and (c) shear to normal stress ratio before, and after 300 bar of depletion. Gray arrows demarcate the depth extent of the dip profile model (the area of stress increase is captured).

3.3.1.5 Criterion for Earthquake Selection

A necessary step in evaluating the rate-and-state model output is to establish a criterion for determining which slip events are earthquakes. This is because, as previously stated, in a rate-and-state model all

points on the fault are always at failure and sliding at a non-zero velocity. Consequently, a minimum slip velocity must be set, above which slip is considered seismic and contributes to the moment release of an earthquake. Coseismic slip velocities are generally thought to be on the order of meters per second (DiToro, 2011) but ruptures in quasi-dynamic rate-and-state models can be slow (Lapusta, 2000) so setting a velocity threshold becomes arbitrary.

The nominal background sliding velocity of the modeled fault is highly dependent on the initial conditions but ranges from $\sim 10^{-21} - 10^{-11}$ m/s. All slip that occurs at a few orders of magnitude above this background rate (10^{-8} m/s) is considered as part of a potential earthquake. The areas of the fault sliding above this minimum threshold velocity are recorded at every time increment. For a 1.5D model, this information can be represented as a 2D matrix, with one dimension representing the spatial position and one dimension representing the time increment. Fault points sliding above the threshold velocity can be stored as “1” and slowly sliding fault points are recorded as “0”. A connected components algorithm can be run to determine areas of “1’s” that are connected in space or time. Each isolated collection of 1’s is an earthquake event and the slip at each of those points is used to determine the earthquake magnitude. The magnitude of the event is calculated as the sum of the total slip multiplied by the fault patch area multiplied by the shear modulus over the slipping fault patch. The maximum sliding velocity of any fault patch, at any time in the event is also recorded. The result is a list of events, each associated with a magnitude and a maximum sliding velocity. Because all of the events above a nominal velocity are recorded it is possible to later filter the data and only examine events above a different sliding velocity. This allows the effect of the choice of threshold value to be examined and determine if the result is dependent on the threshold set.

3.3.2 Earthquake Cycle Model Results

3.3.2.1 Example of Model Results

Once an initial shear stress distribution is determined, a stress history is chosen, and other parameters are selected, the earthquake cycle model is run and an earthquake catalog is generated. Figure 19 and Figure 20 are examples of the catalog created for the strike profile geometry, the aging law, methodology A and a constant shear stress rate. The parameters chosen for this model run are: $a = 0.015$, $a - b = -0.004$, $\bar{\sigma} = 300 \text{ bar}$, $\tau_{mean}^0 = 100 \text{ bar}$, $\tau_{dev}^0 = 25 \text{ bar}$, and $h^*/h = 8$. The initial mean shear stress is far from failure but with the shear stress heterogeneity there are isolated fault patches that are highly stressed and start to slip quickly early on. However, if individual patches start to slip quickly the h^*/h ratio imposed keeps them from slipping quickly enough to be considered an event until enough fault patches start to slip together. Since connected fault areas need to reach failure, and not just one fault patch, it takes a finite amount of time before the shear stress level is increased enough for events to occur.

Figure 19a illustrates the magnitude time history of events and Figure 19b illustrates the area of the fault plane that slipped during each event for a single catalog. Rather than examining individual events, an alternate representation is to look at the cumulative catalog. Figure 20a is the cumulative seismic moment released and Figure 20b is the cumulative number of events. It is also possible to look at the Gutenberg-Richter distribution for the earthquake catalog (Figure 20c). The catalog does not have the characteristic Gutenberg-Richter constant negative slope, of approximately 1.0, that spans several magnitudes. This is

not surprising given that this model is one realization of a fault and does not capture all aspects of the natural earthquake process. Additionally, since the model is a 1.5D representation it cannot fully capture the true complexity found in the earth. However, since the goal of this analysis is to compare the characteristics of earthquake catalogs with different stress histories it is not necessary to fully reproduce the natural world.

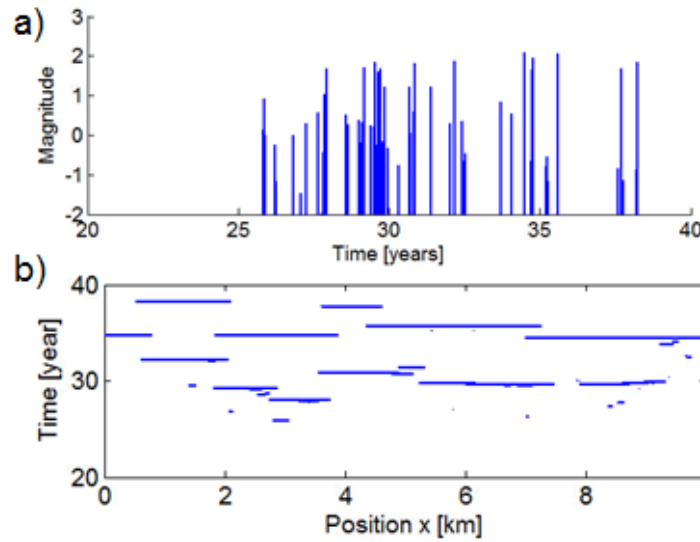


Figure 19. (a) Example of a magnitude time history of events from a simulated catalog. (b) Example of the spatial position of the events in (a). Each horizontal line is the lateral extent of an earthquake

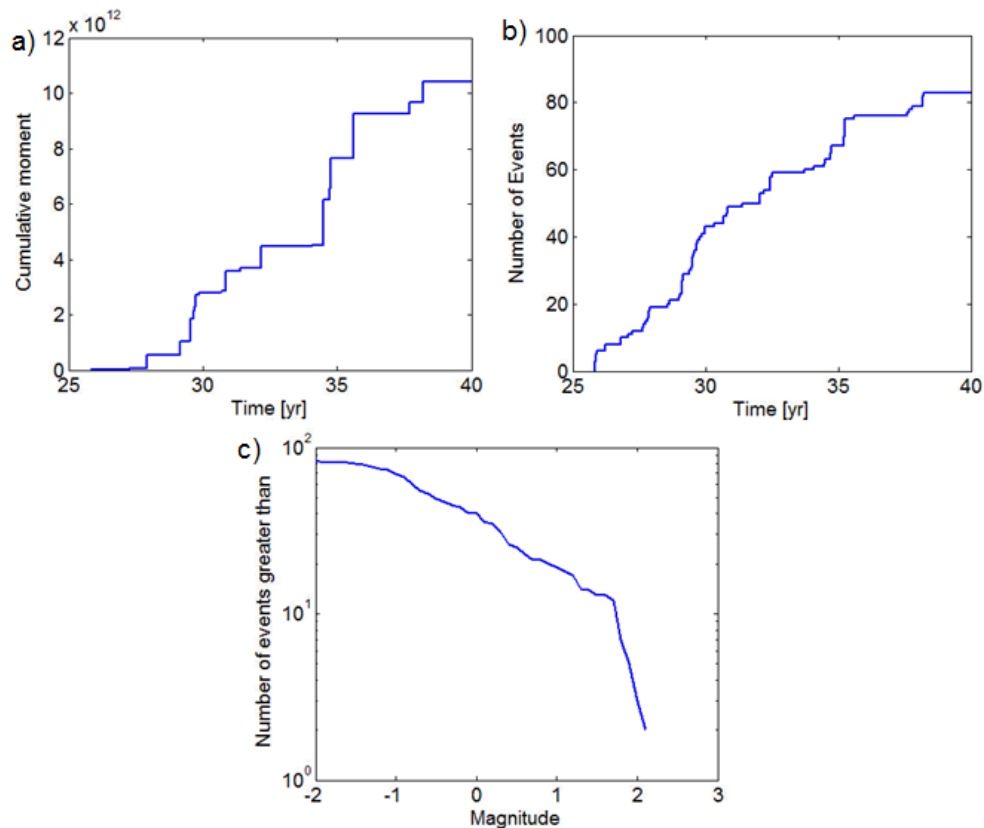


Figure 20. Cumulative effect of the earthquake catalog (a) cumulative moment release, (b) cumulative number of events and (c) Gutenberg-Richter distribution

For this earthquake catalog, after approximately 32 years the majority of the fault has slipped at least once (horizontal lines in Figure 19a have spanned the bulk of the fault). After a portion of the fault slips, the initial stress heterogeneity is removed and the slipped portions of the fault have a relatively uniform shear stress level. This means that while the fault is not at a homogenous stress state, there is no longer an abundance of low shear stress areas that can act as barriers to propagating slip. This stress distribution makes it difficult to stop small events from becoming large and consequently the second half of the catalog has more large events and fewer small events. This loss of shear stress complexity is an artifact of the setup of the problem. Because the shear stress distribution after natural, or induced events should be heterogeneous, the results prior to year 32 are valid and the results post year 32 are controlled by an artifact and are not considered.

3.3.2.2 Effect of Velocity Threshold

Each of the events shown in Figure 19 and Figure 20 has a corresponding maximum sliding velocity. Some events never approach a coseismic sliding velocity (~ 1 m/s) and the slip occurs at low velocities representative of fault creep. Figure 21 illustrates the maximum sliding velocity of each event in 91 different earthquake catalogs (each generated by the same parameter choices as the catalog shown in Figure 19 and Figure 20, but for a different initial realization of stress heterogeneity). All sliding that occurs at a velocity greater than $1e-8$ m/s is preserved from the model run, but only a fraction of these events reach high sliding velocities. There is a clear bimodality to the velocity distribution so an alternate threshold velocity of $1e-2$ m/s is chosen since it separates these populations.

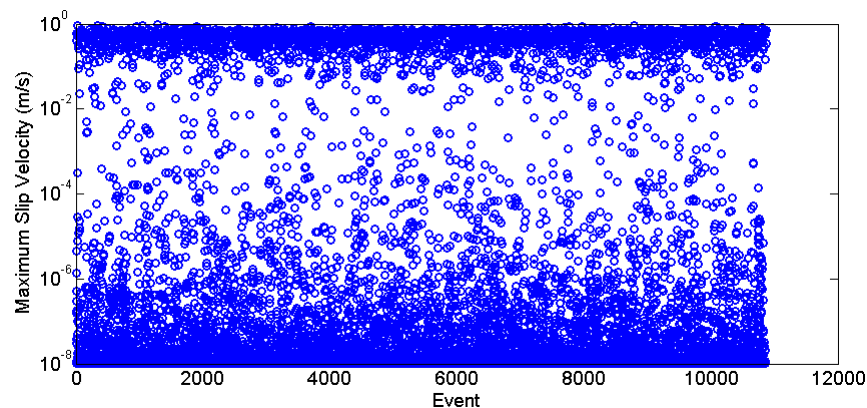


Figure 21. Maximum sliding velocity reached by each event of 91 simulated earthquake catalogs. A threshold velocity of $1e-2$ m/s separates the two distributions

Figure 22 and Figure 23 illustrate the effect of this new threshold on the simulated catalog. The events previously shown in Figure 19 have now been color coded so that events with a minimum threshold velocity of $1e-8$ m/s are plotted in blue and those with a threshold velocity of $1e-2$ m/s are plotted in pink. Where a pink line is visible, there is a blue line underneath it; where a blue line can be seen, there is no pink line and it means that the event occurred with a maximum sliding velocity less than $1e-2$ m/s. If a slightly higher threshold of $1e-1$ m/s is chosen, then an additional two earthquakes are excluded from the final catalog.

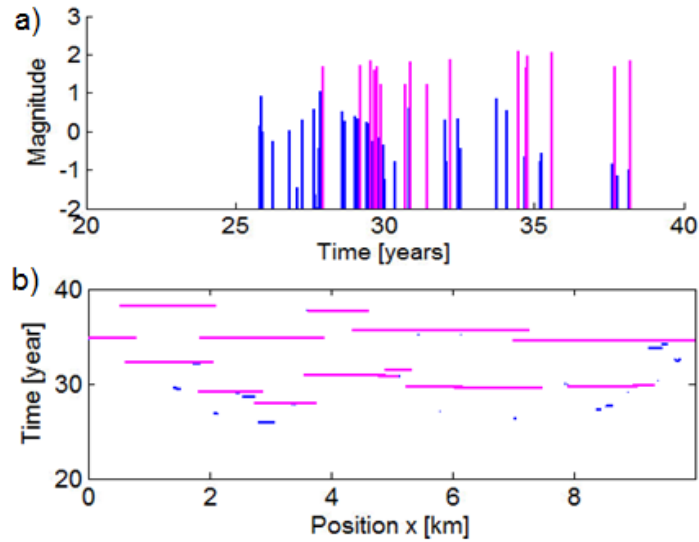


Figure 22. Same model run as shown in Figure 19 but highlighting the effect of threshold velocity on the preserved earthquake catalog. The events with a minimum threshold velocity of $1e-8$ m/s are plotted in blue and those with a threshold velocity of $1e-2$ m/s are plotted in pink. Where the pink line is visible, there is a blue line directly below it; where the blue lines can be seen it is indicative of the fact that that event occurred at a low velocity. (a) time-magnitude history and (b) position-time history.

The largest events happen at the fastest sliding velocities. Many of the initial events occur at low velocities as some of the highest shear stress areas start to slip. These are the result of localized areas of high shear stress surrounded by areas with a sufficiently low shear stress that rupture is unable to breakthrough and accelerate to a faster sliding velocity. As a result, only a small amount of slip occurs and the magnitude of the associated event is small.

Increasing the minimum threshold eliminates all of the small magnitude events. The effect of the minimum threshold velocity on the cumulative moment release of the model is relatively small (Figure 23a) but the effect on the number of events is very large (Figure 23b). Many events occur at low sliding velocities but due to their small magnitude they are only a minor contribution to the energy budget. The effect of velocity thresholding on the catalog is also clearly seen in the Gutenberg-Richter plot in Figure 23c. Most of the following results will be presented for the low threshold velocity of $1e-8$ m/s with the knowledge that increasing the threshold velocity causes the Gutenberg-Richter plot to level off at the small magnitude end.

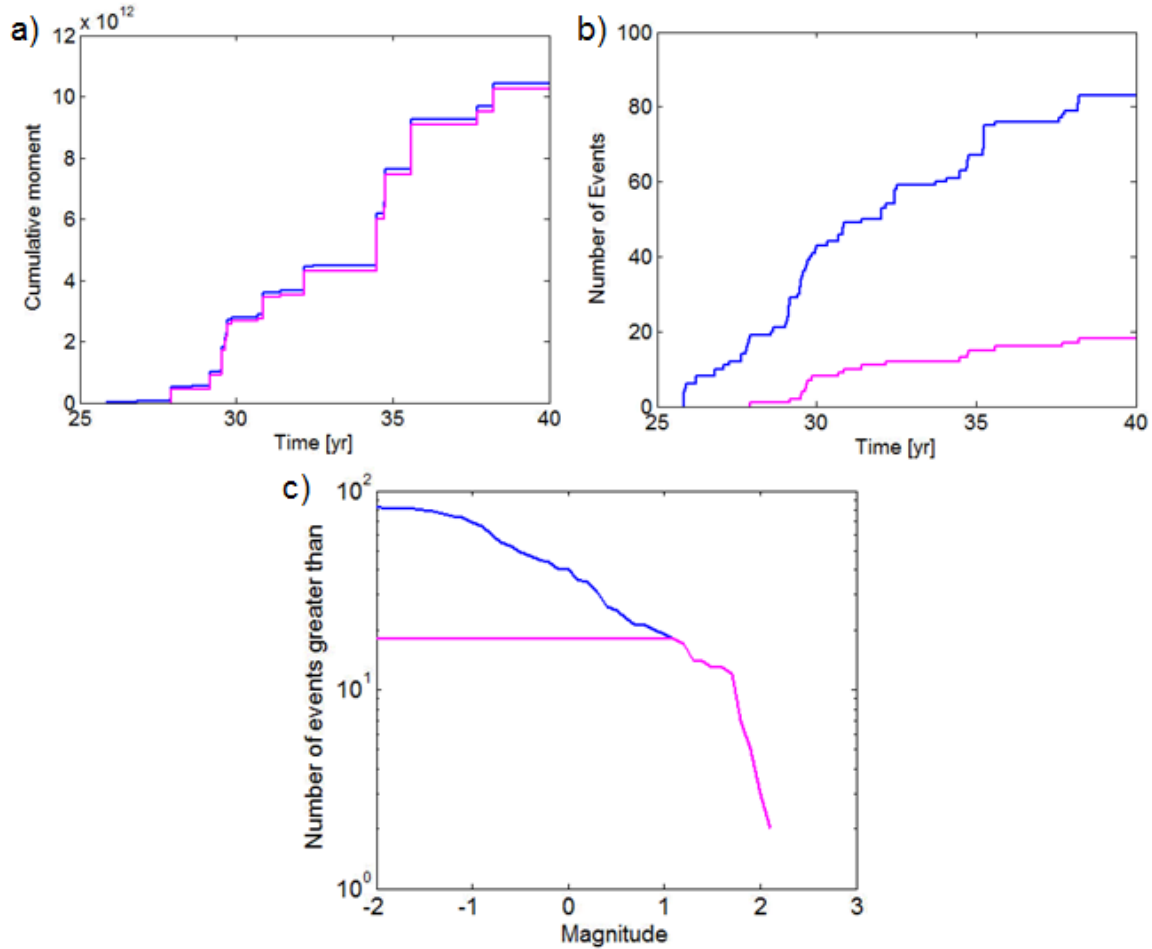


Figure 23. Same model run as shown in Figure 20 but highlighting the effect of threshold velocity on the preserved earthquake catalog. The events with a minimum threshold velocity of $1e-8$ m/s are plotted in blue and those with a threshold velocity of $1e-2$ m/s are plotted in pink. The low velocity events are numerous but low in magnitude and do not substantially contribute to the moment release.

3.3.2.3 Effect of Stress History

The stress history alters the earthquake catalog. Figure 24 and Figure 25 illustrate how the catalog can be altered by the production scenario. The figures represent two different initial shear stress distributions subjected to the three shear stress histories shown in Figure 16. These catalogs were all created by the same model geometry and set of parameters: the strike profile geometry, the aging law, methodology A, a constant shear stress rate, $a = 0.015$, $a - b = -0.004$, $\bar{\sigma} = 300 \text{ bar}$, $\tau_{mean}^0 = 100 \text{ bar}$, $\tau_{dev}^0 = 25 \text{ bar}$, and $h^*/h = 8$. The slight variations in shear stress history result in slight differences in the sliding velocity and state variable evolution. These differences result in slightly different earthquake propagation and magnitude once the next event is triggered.

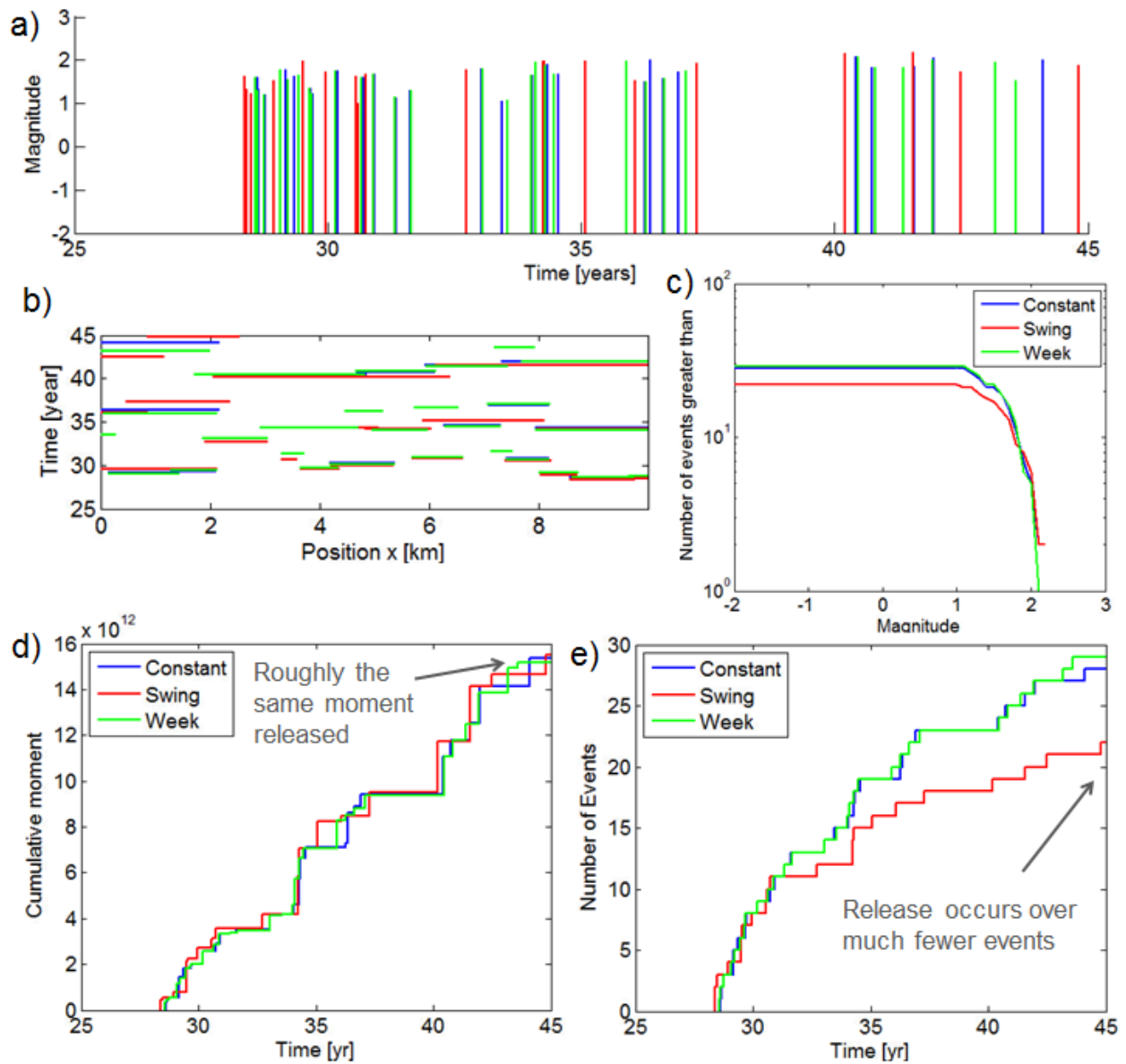


Figure 24. Example effect of stress history on the earthquake catalog for one initial shear stress distribution. The same model initial condition (shear stress distribution) was subjected to three time histories. (a) Magnitude-time history plot, (b) Position-history plot, (c) Gutenberg-Richter plot, (d) Cumulative moment release and (e) Cumulative number of events. A minimum threshold velocity of $1e-2$ m/s was applied to each catalog.

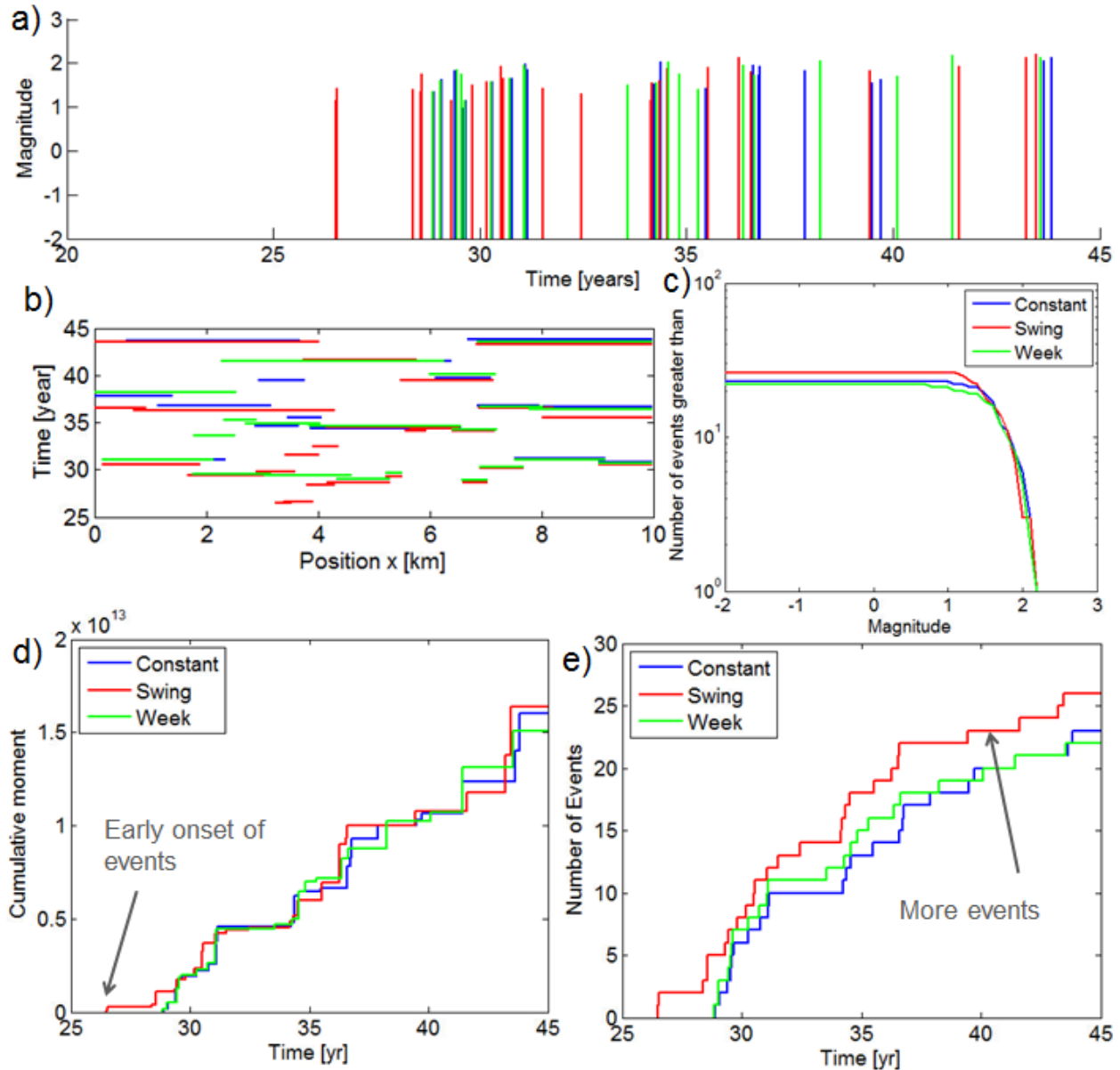


Figure 25. Example effect of stress history on the earthquake catalog for a different initial shear stress distribution to that shown in Figure 24. The same model initial condition (shear stress distribution) was subjected to three time histories. (a) Magnitude-time history plot, (b) Position-history plot, (c) Gutenberg-Richter plot, (d) Cumulative moment release and (e) Cumulative number of events. A minimum threshold velocity of $1e-2$ m/s was applied to each catalog.

The example shown in Figure 24a and b illustrates the slight differences in timing, position and magnitudes of events that occur. A minimum threshold velocity of $1e-2$ m/s is used for easier visual comparison of events by eliminating the smallest earthquakes from the catalogs. Sometimes the same event occurs in all stress histories but often there are small variations in the timing and lateral extent. The sequence of earthquake events is highly influenced by the initial shear stress distribution so there is a high degree of similarity among the catalogs. Figure 24d and e show that approximately the same amount of cumulative moment was released in the three history scenarios, but the seasonal swing production scenario released

the moment over many fewer events in this simulated catalog. This indicates that the seasonal swing scenario had a larger average event size than the constant production or weekly variability scenarios. In contrast, the results shown in Figure 25 for a different realization of initial conditions show a very different result. Figure 25d and e show that the seasonal swing scenario releases approximately the same moment over many more events, implying a smaller average earthquake magnitude. In this example the seasonal swing scenario also has a slightly earlier initial onset time for the earthquakes.

The conflicting results shown in Figure 24 and Figure 25 illustrate the importance of examining many simulated earthquake catalogs for each of the production histories being evaluated. Any individual realization will have an insufficient number of earthquakes to draw conclusions about the general effect of the production history on the earthquake catalog. Consequently, for a given unique model setup many realizations of different initial shear stress distribution must be run to ensure that the conclusions are not influenced by an insufficiently large data set. These are then compared, in aggregate, for the various stress history scenarios. Using this methodology it is possible to determine if there is any statistically significant effect on the associated seismicity.

3.3.2.4 Aggregated Catalogs

It is not possible to draw conclusions from any individual earthquake catalog realization because the results are highly dependent on the initial conditions. Therefore, to determine if the stress history has an effect on the character of the earthquake catalog many realizations are run and the individual earthquake catalogs are compiled into one aggregate catalog. This can be interpreted as the summation over many faults in a field or as an average fault behavior.

Once the catalog is compiled it is no longer informative to examine individual earthquake events so figures like Figure 24a and c are not generated for comparison. Instead, attention is focused on the cumulative moment, cumulative number of events, and the Gutenberg-Richter plots. Figure 26 shows the compiled results from $N=91$ catalog realizations with a minimum threshold velocity of $1e-8$ m/s. This means that 91 different initial shear stress distributions were examined and each initial condition was run three times, once for each of the three stress histories examined.

Figure 26a shows the timing of the events throughout the year. The imposed seasonal swing signal is clearly recovered from the model simulations. Similar to the simplified Dieterich activity rate model discussed in section 3.2 (and the observed Groningen earthquake catalog) there is a phase delay between the time of highest stressing rate and the time of the most earthquakes. The imposed signal is a sinusoid with a peak stressing rate a quarter of the way through the year (April 1) but the peak earthquake activity is centered around June and July. There is no substantial difference in the shear stress history throughout the year for the constant or the weekly variation scenario so there is a relatively constant level of earthquake occurrence in each month for these scenarios. When only one catalog per stress history is examined, the seasonal differences between the history scenarios are not evident. Only when many catalogs are examined in aggregate does the signal become clear.

Figure 26b shows the aggregate moment release in all of the models. Due to the combination of 91 catalogs the stair step nature of the curves is not as apparent as it is in Figure 24 and Figure 25. The

relative smoothness of the curves makes the data easier to interpret because they are no longer dominated by the large jumps of the largest events. In the enlarged section of the plot the seasonal nature of the “swing” case is readily apparent with more moment released during the middle of the year due to the increased activity. This picture looks remarkably similar to the forcing shown in Figure 16b (with a phase shift). However, even with this seasonal shift, at the end of each cycle the cumulative moment is nearly identical for the three stress history scenarios.

Figure 26c shows the Gutenberg-Richter plots for all of the years and for just the events that occurred in year 32 or earlier. The largest events occur after year 32 and there are fewer events in the catalog when only the events occurring in or before year 32 are considered. Regardless of the timeframe examined, the three stress scenarios overlie one another in the Gutenberg-Richter plot. This indicates that there is no significant difference in the character of the seismicity as a result of the stress history.

Figure 26d shows the cumulative number of events for each stress history scenario. There is a clear break in slope at year 32 due to the fact that by the end of year 32 the most of each fault has slipped at least once. As discussed in section 3.3.2.1, this results in a loss of stress heterogeneity so there are few low stress barriers to stop the event propagation. The moment release rate is relatively constant from year 27-50, demonstrating that even though fewer earthquakes are occurring they tend to be larger events. After year 32 there is some divergence between the three scenarios in Figure 26d but this is driven by only the slowest sliding velocity events. If the threshold velocity is increased to $1e-2$ m/s, the spread in these lines is greatly diminished and the curves in Figure 26b nearly overlap one another. Additionally, the seasonal swing signal can still be observed in Figure 26a, although the earthquake count is decreased. As discussed previously, the loss of stress heterogeneity is an artifact of the model and in a natural setting heterogeneity would be preserved (e.g. geometrical roughness is responsible for some heterogeneity and that does not disappear after an earthquake). For this reason the results post year 32 are not considered valid.

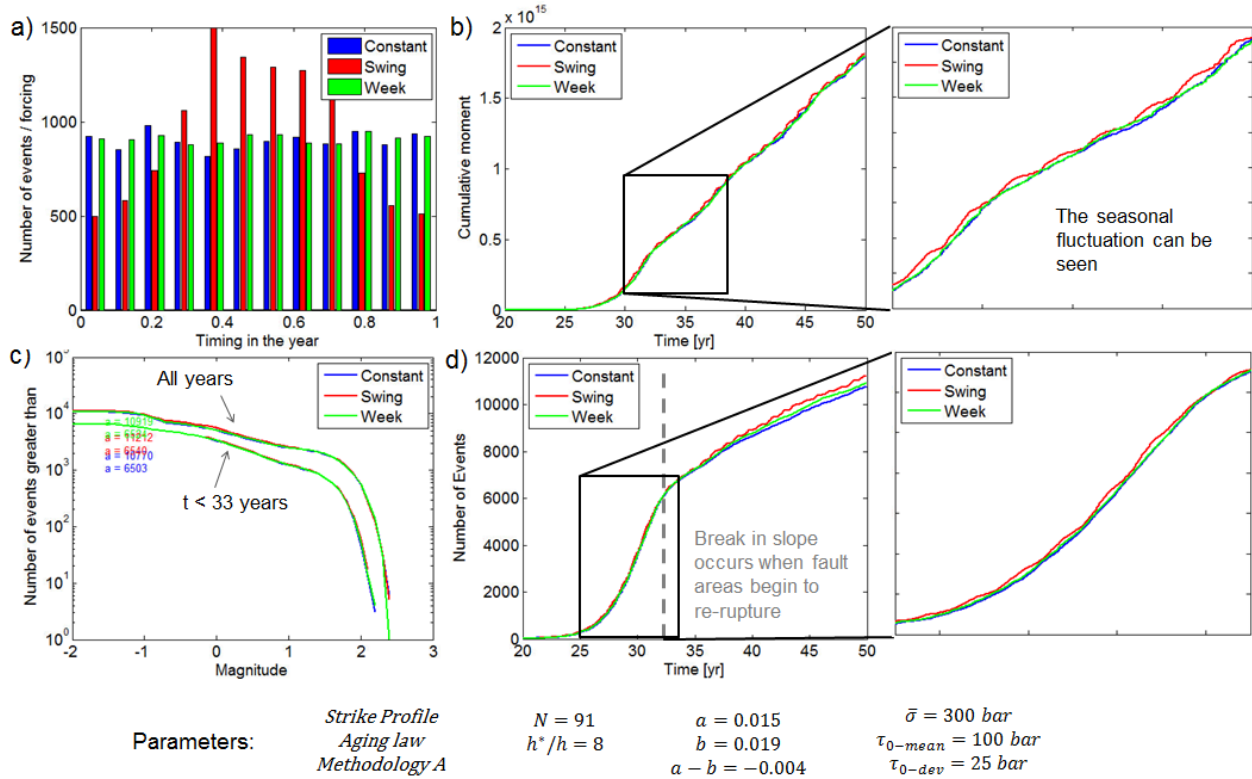


Figure 26. Aggregate earthquake catalog from 91 separate realizations of initial stress conditions. (a) the seasonal swing signal is clearly observable in the monthly occurrence of earthquake events, (b) all three stress scenarios accumulate moment at approximately the same rate with some variation due to the seasonal swing, (c) Gutenberg-Richter plot of all events in the aggregate catalog and just those that happened prior to Jan 1 of year 33, (d) all three stress scenarios have a similar cumulative number of events, with some modification for the seasonal swing scenario.

In aggregate the modeled earthquake catalog indicates that there is no significant difference in the character of the seismicity as a result of differences in the stress history. When considered individually some realizations of the earthquake catalog do contradict this conclusion but any individual realization of the earthquake catalog is highly dependent on the initial random shear stress distribution. Unfortunately, since all the distributions have the same characteristics it is not currently possible to determine which particular initial condition is the most representative of a given Groningen fault. Since no most representative shear stress distribution can be identified, it is not reasonable to evaluate individual earthquake catalogs in isolation and the aggregate catalog must be considered in order to insure that the conclusions reflect the system behavior.

These model results do not support the statement that swings or fluctuations in production alter the seismic hazard compared to a constant production scenario. These model results support the idea that while there may be a shift in the timing of earthquakes due to the production schedule, if the same amount of gas is produced over a timeframe, the hazard during that time is unchanged by the production schedule.

3.3.2.4 Model Scenarios Examined

The results presented in section 3.3.2.3 were for one fault geometry, one set of input parameters, one rate-and-state evolution law and one methodology for bringing the fault to failure. The effect of these choices must be examined to determine if there are other model scenarios that alter the conclusion that seismic hazard is not affected by production schedule.

Model Input Parameters

While keeping with the methodology and geometry of the previous section it is possible to examine the effect of some of the basic parameters that were specified. The degree of initial stress heterogeneity, the rate-weakening behavior and the model resolution were all modified to evaluate their impact on the resulting earthquake catalogs.

In the previous section, the degree of initial shear stress heterogeneity was assumed to be $\tau_{dev}^0 = 25$ bar. Aggregate catalogs have also been examined with $\tau_{dev}^0 = 15$ and 35 bar without a change to the conclusions. In the case of $\tau_{dev}^0 = 15$ bar there was less stress heterogeneity and some of the early events were larger because of fewer stress barriers to stop rupture propagation. For a higher degree of stress heterogeneity the earthquakes were smaller since there were many low stress areas to stop rupture propagation. However, regardless of these changes in the earthquake catalog, there was no significant difference between the three stress histories examined.

Prior results implemented a rate-weakening behavior characterized by $a = 0.015$ and $a - b = -0.004$. The case of $a - b = -0.008$ has also been examined with no change in the conclusions.

The resolution of the problem was also modified by changing the size of h^* so that $h^*/h = 16$. This specification changes the length of L_f by a factor of 2 and doubles the critical size (the patch size capable of failing independently). The result of this modification was to decrease the number of the smallest magnitude, low velocity events. Conversely, a modification such that $h^*/h = 4$ increased the number of small events. This parameter choice has a large effect on the seismicity, but there was still no statistical difference between the three stressing scenarios.

Stress History

Applying a phase shift to the seasonal swing modifies the shear stress history as shown in Figure 16c. This allows the cumulative shear stress for the seasonal swing scenario to be both larger and smaller than the constant stress rate scenario, here called a “centered case” (Figure 16c). Additionally, it is also possible to increase the amplitude of the swing in the shear stress rate so that the stress is not monotonically increasing. As discussed in section 2, at most distances from a production well the pore pressure field is predominantly monotonically decreasing, but near producing wells the pore pressure may increase as well as decrease as a result of the production schedule. Therefore both monotonically and non-monotonically increasing shear stress scenarios are examined.

The aggregate results are presented with a minimum threshold velocity of $1e-8$ m/s in Figure 27 and $1e-2$ m/s in Figure 28. The deviation that occurs after year 40 in Figure 27c is not present in Figure 28c indicating that the difference in the number of events is the result of the slow, small magnitude events

only. However, changing the velocity threshold does not alter the conclusion that production history does not affect the character of the seismicity.

In the non-monotonic case there is a large amount of variation throughout the year due to the fact that stresses increase quickly followed by times of decreases in stress which decrease earthquake activity. However, consistent with previous results, there is no statistically significant effect of the production history on the character of the earthquake catalog for a case of non-monotonically increasing shear stress history. Even large differences in stress history, including both loading and unloading of the fault, do not suggest that production fluctuations alter the seismic hazard.

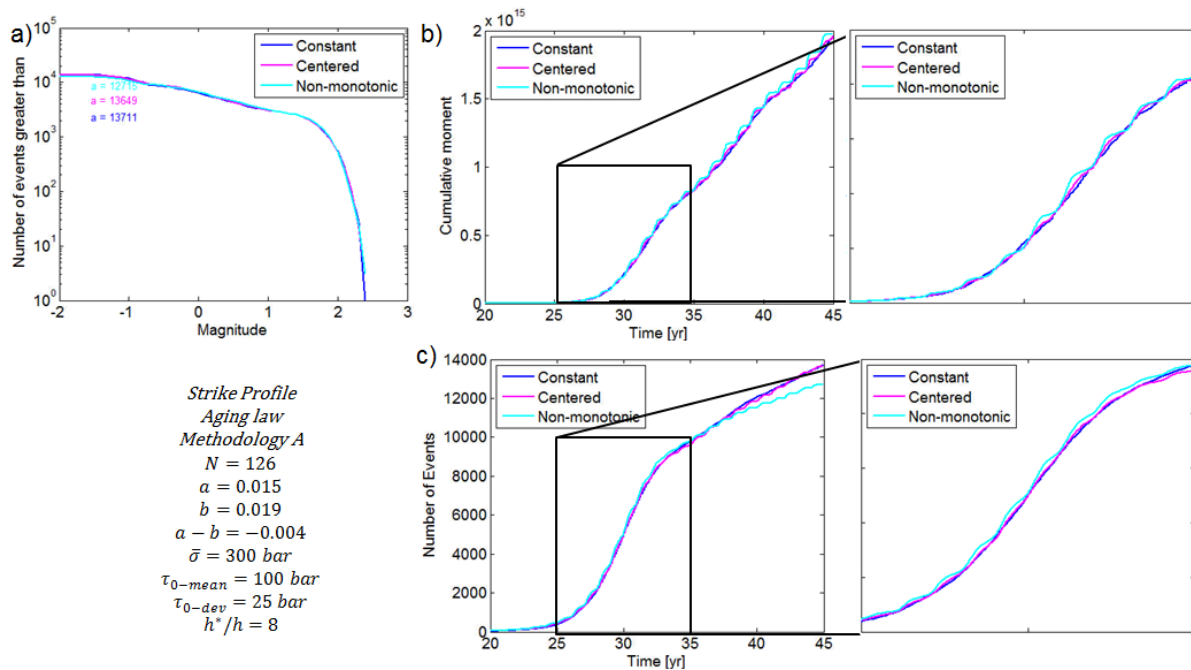


Figure 27. Similar to the results shown in Figure 26 but for different shear stress histories. (a) Gutenberg-Richter plot, (b) aggregate cumulative moment over time, and (c) aggregate total number of events over time. The shear stress histories used to generate these scenarios are shown in Figure 16c. Minimum threshold velocity of $1\text{e-}8 \text{ m/s}$ was applied.

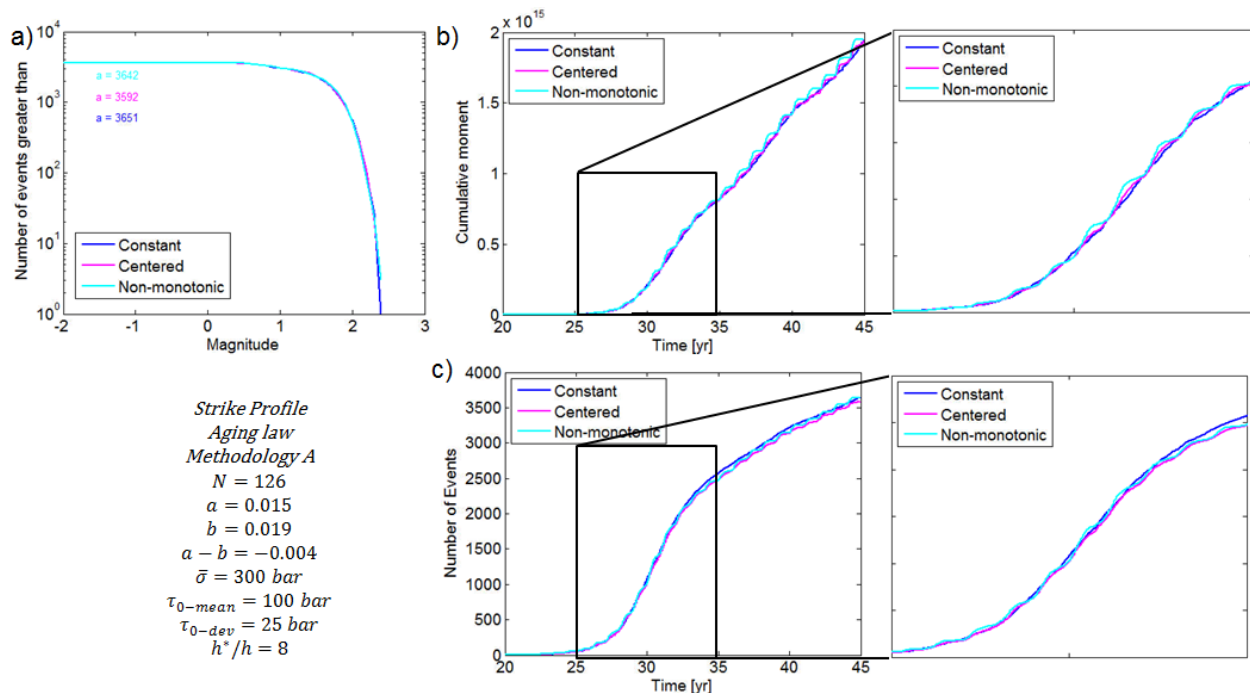


Figure 28. Same as Figure 27 but for a minimum velocity threshold of 1e-2 m/s. Changing the velocity threshold does not alter the conclusions

State Variable Evolution Equation

All results presented so far have used the Aging law for the state variable evolution and have had a constant normal stress during the earthquake cycle (methodology A). The Slip Law, like the basic implementation of the Aging law, is insensitive to variations in normal stress. This law was also examined, in conjunction with methodology A, to determine how this would affect the model results.

The aggregate results are presented in Figure 29 with a minimum threshold velocity or 1e-8 m/s. It is clearly observed in Figure 29c that there are a large number of events that occur early in the model run as the initially high shear stress locations slip. However, the cumulative moment released in these events is very small (Figure 29b). A larger minimum threshold velocity (1e-2 m/s) decreases the number of early events but does not eliminate them. In general, the slip law allows for faster slip velocities over small patch sizes, but only a small amount of slip accumulates during these events.

Implementing the Slip Law significantly changes the resulting modeled earthquake catalog, but even with this rather large change there is no change in the conclusion: the character of the seismicity is not affected by different stress histories.

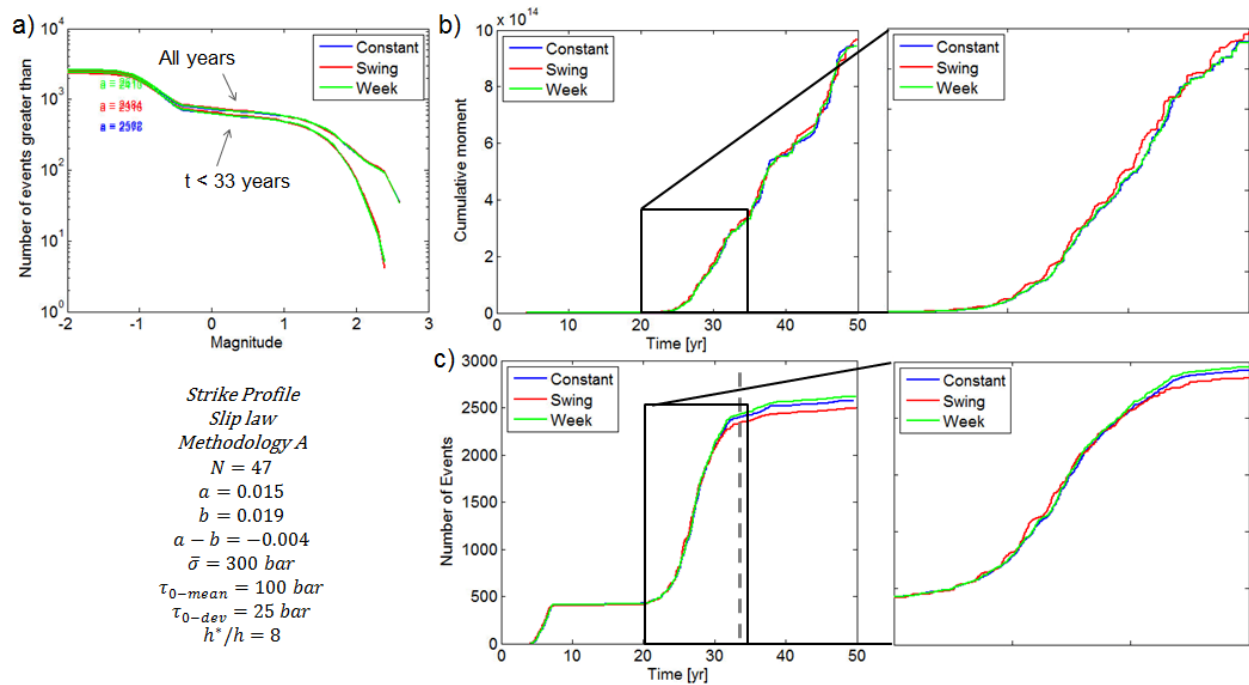


Figure 29: Similar to the results shown in Figure 26 but for the Slip Law state variable evolution equation. The same shear stress histories were applied to the models presented in Figure 26 and the results shown here. (a) Gutenberg-Richter plot, (b) aggregate cumulative moment over time, and (c) aggregate total number of events over time. A minimum threshold velocity of $1e-8$ was applied.

Methodology B with Normal Stress Dependence

Methodology A neglects changes in normal stress which can be significant in the case of oil and gas activity. In contrast, methodology B accounts for variable effective normal stress and implements the Aging form of the state variable evolution equation with the third term that incorporates normal stress dependence. Utilizing this relationship allows for the effect of normal stress variations to be evaluated. The cases of constant, monotonically increasing and non-monotonically increasing stress histories are all examined. The shear and effective normal stress evolution is solved for based on imposed pore pressure changes and is specified as $\Delta\tau_{mean}^0/\Delta P_p$ and $\Delta\bar{\sigma}/\Delta P_p$.

Figure 30 shows the comparison of the three scenarios examined. In blue is the case of constant production rate and no normal stress dependence (similar to all results presented previously with $\alpha = 0$), in orange is the case of constant production rate and including a normal stress dependence ($\alpha = 0.5$) and in light purple is the case of seasonal swing production, phase shifted so that it is centered over the constant rate and with a large amplitude such that both the normal and shear stress changes increase non-monotonically (stress history scenario is light blue in Figure 16c). Due to the slower rate of stress increase as compared to methodology A, events do not begin until much later than in the previous examples presented. However, similar to previous results the seasonality signal is clearly visible in Figure 30a. The results in Figure 30b and c overlie one another indicating that there is no difference in the character of the seismicity when changes in normal stress are included. Additional values of α were also considered ($\alpha = 0.8$ and 1.0) with no change in the conclusions. Finally, constant and non-monotonic fault loading also do not result in different seismic hazards.

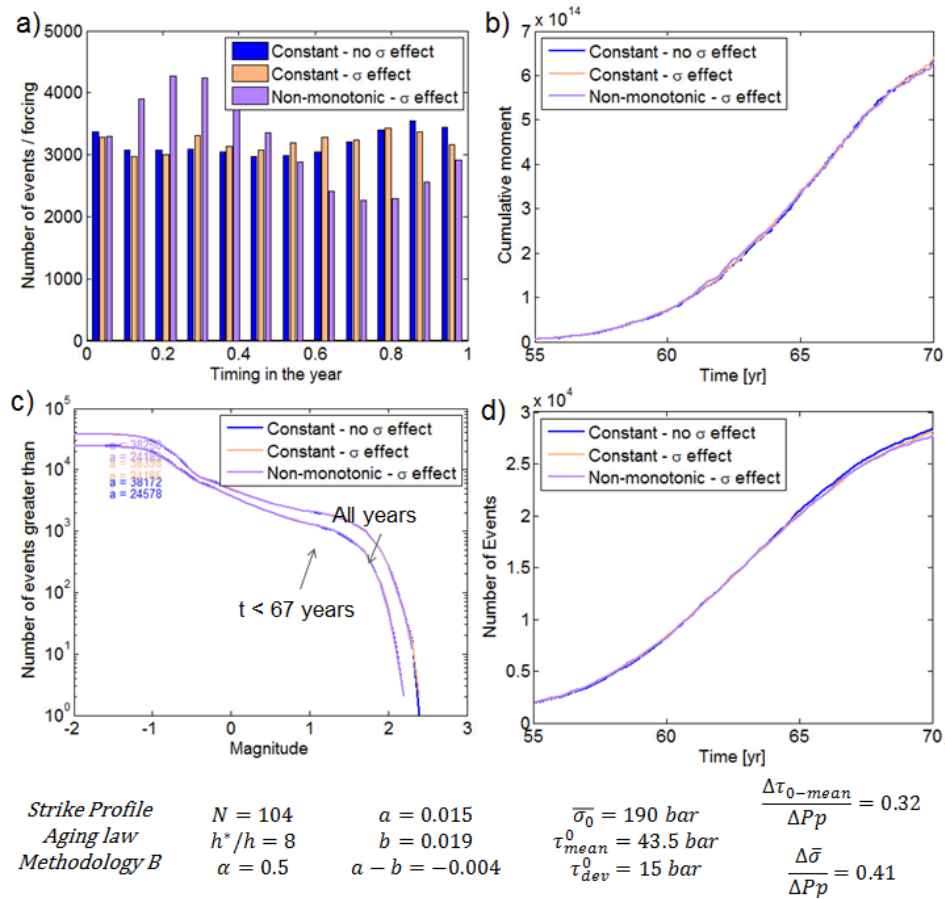


Figure 30. Similar to Figure 26 but for the Aging law and the inclusion of normal stress changes and dependence.

Methodology C with Dip Profile Geometry

The results presented in the previous sections were all for a strike geometry and for a uniform increase in stresses across the entire fault. Methodology C implements a position dependent loading history, as described in section 3.3.1.3, with a dip profile geometry. The imposed preexisting fault throw leads to areas of both increased and decreased loading as a result of homogeneous pore pressure depletion. An ABAQUS finite element model is used to solve for the position dependent changes in shear and normal stresses, as a function of depletion, and these stress changes are used to drive the rate-and-state model to failure. Since normal stress changes are included, the Aging law with a normal stress dependence and a value of $\alpha = 0.5$ was used.

The stress evolution is dependent on the amount of fault offset so five fault offsets were considered (25, 50, 100, 150 and 175 m) of a 200 m thick reservoir. The results for a fault offset of 100 m are presented in Figure 31 and are representative of all fault offsets considered. Similar to all previous results presented, there is no significant change in the character of the seismicity due to the stress history.

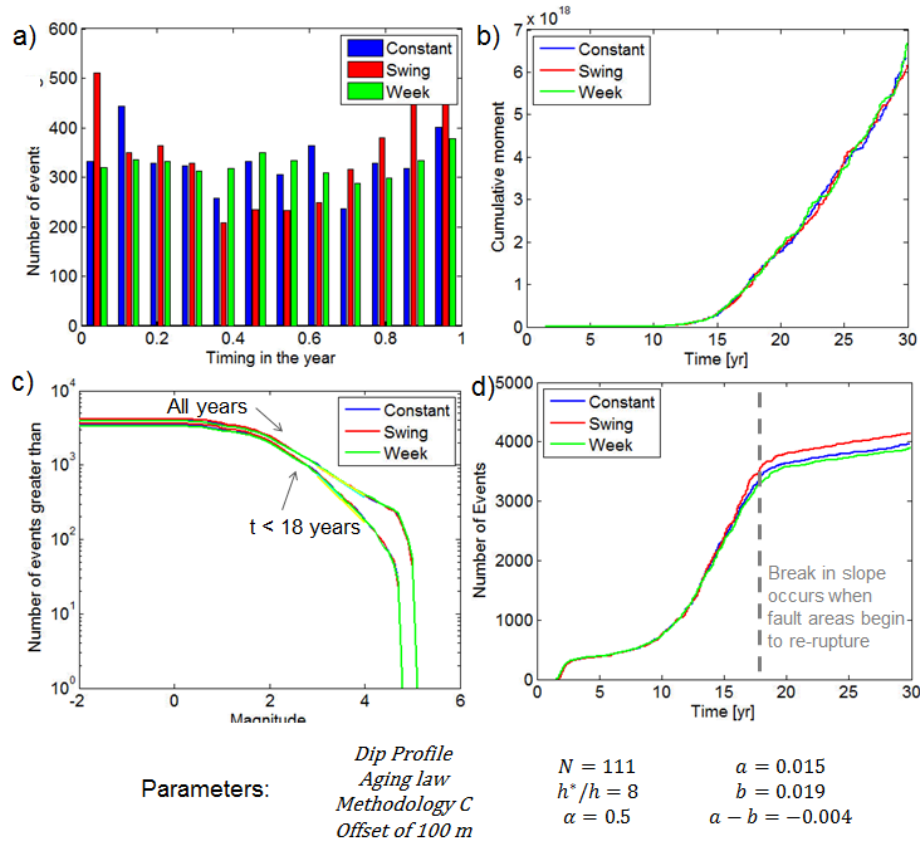


Figure 31. Same as Figure 26 but for a dip profile geometry with 100 m of fault offset. A minimum velocity threshold of $1e-2$ m/s was applied.

3.3.3 Earthquake Cycle Model Conclusions

An earthquake cycle model implementing rate-and-state friction was used to examine the effect of fluctuations (or swings) in production on simulated earthquake catalogs. The model does not explicitly solve for the pore pressure and stress fields due to production but rather uses the effect of a pore pressure change on the stress field to examine the history of earthquakes on a fault. Pore pressure changes result in shear and normal stress changes and those stress histories are specified as boundary conditions to the problem. Some models were simplified to neglect normal stress changes, some models assumed uniform stressing over the entire fault, and some captured position dependent stress histories and normal stress changes. None of these variations in approach alter the conclusions of the study.

To determine if variations in production schedule can be expected to alter the character of the seismicity, the same model initial conditions were used to solve for an earthquake catalog under three stress history scenarios: 1) constant production rate, 2) seasonal swing production and 3) 1 week on and 3 weeks off. The same amount of gas is produced in each scenario so the final state of stress is the same for these three scenarios. Any one set of initial shear stress conditions may result in earthquake catalogs that would drive a conclusion that one scenario is “worse” for seismicity than another. Therefore many simulations were examined in aggregate to determine if there is a statistically different character to the seismicity under the three stress histories. This modeling study finds that in aggregate there is no difference

between the three scenarios. The total production affects the amount of seismicity but the path to that production was not found to have an effect on the hazard in the model.

The models were 1.5D representations of faults (i.e. a 2D fault surface was discretized into fault patches in either the strike or dip direction) capturing either along strike propagation or down-dip rupture propagation. The fault dimension in the other direction is a specified finite number. Fully 2D representations of fault surfaces were also performed, but the computational demands were too high to prove useful given the large number of realizations necessary to generate useful results for this study.

There are several forms of rate-and-state friction and many parameter choices need to be made for a simulation. This study examined variations in

- Initial shear stress heterogeneity
- Normal stress dependence
- State variable evolution law (Slip law and Aging law, with and without normal stress dependence)
- Degree of rate weakening ($a - b$ value)
- Critical patch size (also affects the rate weakening slip distance L_f)
- Velocity threshold for determining if an earthquake has occurred
- Strike and dip geometries
- Uniform and position dependent stress evolution
- Monotonic and non-monotonic increases in fault loading

The results of all variations were consistent with one another. The stress history does alter the simulated earthquake catalog but when multiple simulations are viewed in aggregate, there is no difference between the stress scenarios. These results show no impact of fluctuations in production on the seismic hazard. No stress history scenario consistently produces larger, and therefore more damaging, earthquakes. These results support the idea that while there may be a shift in the timing of earthquakes due to the production schedule, if the same amount of gas is produced over a given timeframe, the hazard during that time is unchanged by the production schedule.

3.4 Geomechanical Modeling Summary and Conclusions

Laboratory tests have revealed that there are properties of friction that are not captured by Coulomb friction because friction is not a constant but rather an evolving quantity. The rate-and-state friction formulation captures the sliding velocity dependent behavior as well as the time (or state) dependent properties of friction. These characteristics make the rate-and-state formulation well suited to address the issue of production fluctuations because the “state” portion of the formulation makes the result dependent on the sliding history of the fault and could allow for differences in behavior based on the production (or stress) history.

A simplified implementation of rate-and-state friction considers only the earthquake occurrence rate and how it is affected by the stress history. The implementation of Dieterich (1995) can be used to reproduce the decay of aftershocks and changes in earthquake rate due to changes in the background loading rate. This model was used to compare earthquake rates and the total number of earthquakes for constant as

well as seasonal and daily fluctuations in shear stressing rate. The same number of earthquakes was found to occur in all the scenarios. The timing of a given earthquake can shift within the time frame based on the loading but the earthquake activity rate model does not suggest that there will be a difference in the aggregate hazard due to fluctuating vs. constant production.

The simplified model was greatly expanded into a full rate-and-state fault friction representation. Coseismic and interseismic times were modeled and the resulting earthquake catalogs were compared for different scenarios. This model is a 1.5D representation of a fault and includes calculations of earthquake magnitudes as well as earthquake frequency. With this capability it is possible to address the question as to whether fluctuations in production result in larger earthquakes or an increased number of earthquakes. Answers to these questions make it possible to determine if a change in the hazard can be anticipated due to fluctuations in production.

Many model parameters and methods of implementation were examined and no model was able to identify an aggregate change in the character of the seismicity due to constant versus fluctuating production. Any individual model realization could lead the observer to conclude that one production scenario is “worse” than another, but when many model realizations are included, there is no statistical difference between the scenarios. Earthquake timing may shift within the year, but there is no change to the expected number of events or magnitude of events expected within a year.

These modeling efforts do not support the statement that fluctuations in production affect the seismic hazard.

4.0 Alternate Lines of Investigation

During the preliminary study, a few lines of investigation were considered that ultimately did not provide any significant insight. A seasonal swing production schedule was incorporated into a 3D fault based geomechanical model and analog case studies from surface reservoir impoundment were considered. For completeness, these studies are included here but no further work or expansion on these topics is underway.

4.1 Static Coulomb Friction Models

4.1.1 Introduction and Model Setup

ExxonMobil URC has used the commercial finite element program, ABAQUS, to develop a quasi-static 3D geomechanical model covering large portions of the Groningen field and including ~90% of the faults mapped in those areas (Lele et al., 2016). The model uses the pore pressures from the NAM internal reservoir simulator to examine the compactive and fault slip behavior of the reservoir rocks. The finite element model imposes pore pressure changes in a global model that does not explicitly include faults (reservoir layers are draped across faults to approximate the pre-existing fault offsets) and extends far beyond the boundaries of the field. The prescribed pore pressures are taken from the reservoir simulation model that is history matched to the production and forecasts future pore pressure changes for different production scenarios. The deformations calculated in this global model are then applied as boundary conditions to three overlapping submodels that cover domains smaller than the field and explicitly include the faults. The faults are modeled as contact surfaces that are able to slide past one another. Figure 32 is an example of the slip magnitude that accumulates on the modeled faults in one of the submodels. The complex geometry (e.g. surface roughness) cannot be fully captured in these submodels, but the spatially variable average strike and dip of the fault are well represented. Both the global model and the submodels have porosity (location) dependent elastic moduli. The porosity variation throughout the field is prescribed by the geologic model and the elastic moduli dependence on the porosity is constrained from lab data.

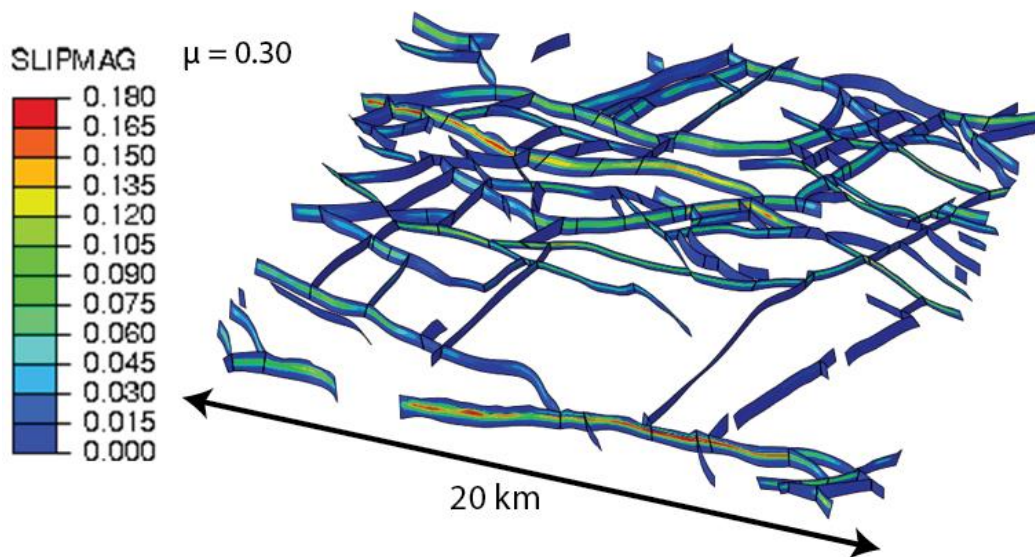


Figure 32. Oblique view of one of three geomechanical submodels. Contoured value is the magnitude of slip for the case of $\mu = 0.30$.

The static model does not explicitly capture earthquakes but it is able to capture when faults are reaching the point of Coulomb frictional slip. In Coulomb friction the stress path taken to reach failure does not affect the failure that occurs, making the onset of failure, path and rate independent. Therefore variations in the stress buildup that would result from constant versus fluctuating production are not expected to substantially modify the failure response of the model.

Once faults in the model reach failure the faults begin to slip at a constant ratio of shear to normal stress (characterized by the coefficient of friction that is specified). This representation does not capture what actually occurs during an earthquake. It is observed that during real earthquakes faults weaken substantially so the shear to normal stress ratio drops and this facilitates additional slip. A geomechanics model with a high coefficient of friction (0.45-0.6) can capture when an area would start to slip, but it will always underestimate the total amount of slip because the dynamic effects of fault weakening are not included. A geomechanics model with a low coefficient of friction will result in faults that start to slip much earlier than expected/actually observed, but the resulting amount of slip would better reflect the amount of slip that could occur if earthquakes were to release the built up stress. These trade-offs are inherent to the model because a static geomechanics model is not reproducing actual earthquake behavior.

The finite element model is driven by the pore pressure histories captured in the NAM reservoir simulator. The reservoir model simulates the pore pressure distribution in the field that results from all the wells (opposed to the single well captured in the analytic solution of section 2.0). This allows for the long term depletion trend to be accurately captured rather than the ad hoc superposition of a depletion trend as shown in Figure 8.

The reservoir simulator output from NAM has been obtained with hourly and monthly outputs of pressure. The lateral cell size in the simulator is slightly larger than 400 m (1300 ft). The lateral element size in the EM global model is ~500 meters and in the sub-models that contain faults the lateral element size is ~100 - 400 meters. Figure 3 shows that a daily production swing of $\pm 100\%$ has negligible impact 300 meters away so the reservoir simulator will show little effect of the daily fluctuations (average change of 0.01% observed). However, the reservoir simulator is able to capture the pore pressure changes due to the fluctuations on the year time scale because the effects of these fluctuations are felt over much larger distances. Section 2.2 showed the results of the analytic solution around one well, but the effect in the reservoir simulator will be different due to the complex heterogeneity that exists in the subsurface and the complicated production rates imposed at the well locations. Additionally, if more production occurs in the North of the field, the reservoir simulator will capture the redistribution of pore pressure from the South to the North due to diffusion across the field.

Figure 33 shows the pore pressure changes in the reservoir model during several one month intervals. There are no areas of pore pressure increase in the area of the geomechanics submodel 1 (black dashed line) but there are some such areas in submodel 2 (red dashed line). Therefore, the faults in submodel 2 will feel some degree of loading and unloading throughout a year, but submodel 1 will not.

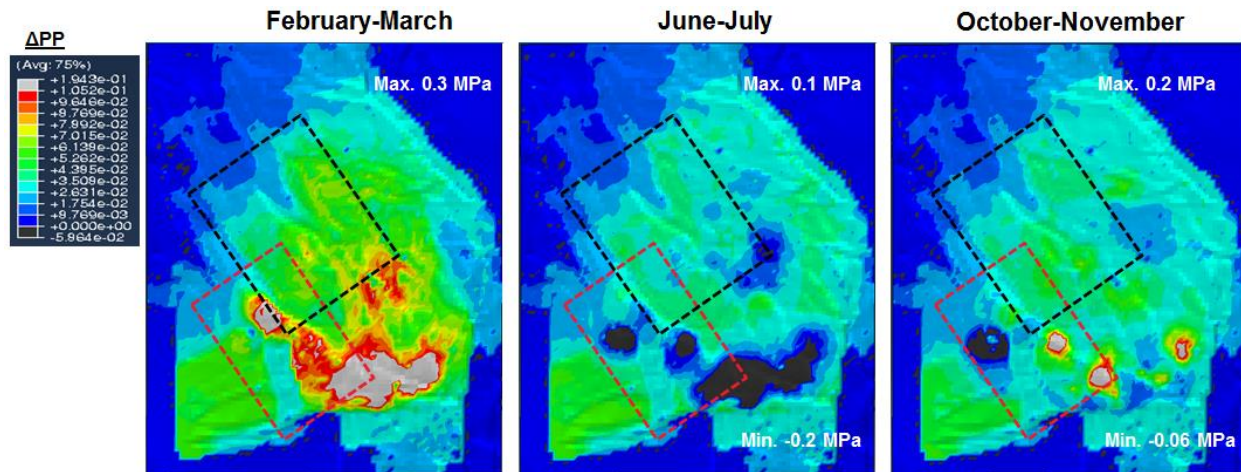


Figure 33. Pore pressure changes from month to month in the reservoir model for 2012. Areas of black are where pore pressure increases. Red outline is the location of submodel 2 and black outline is the location of submodel 1. There are no areas of pore pressure increase in submodel 1 but there are some areas in submodel 2.

4.1.2 Static Model Results

The pore pressure changes from the reservoir simulator are imposed and the geomechanics model responds with volumetric and shear deformations and slip on the fault surfaces. Several metrics of fault based deformation can be examined (slip (i.e. moment) or energy), and here the dissipated energy is presented. The dissipated energy is the integral over all the fault areas of slip*shear stress. Given the magnitude and lateral extent of pore pressure disturbances due to daily fluctuations, the geomechanics model will not show a response to these oscillations. However, the oscillations on the year time scale are felt throughout the field and can be captured by the static geomechanics model.

Two geomechanics model runs were made. The first assumed constant production throughout the year. The second incorporated production fluctuations over the course of the year, using reservoir simulators monthly pore pressure values for the 2012 calendar year. In both submodels a variation in the dissipated energy per month can be seen between the two production scenarios (Figure 34). There is an increase in dissipated energy during months of high production but the cumulative difference at the end of one year is negligible between the constant and variable production scenarios (0.008% of submodel 1 and 0.18% for submodel 2).

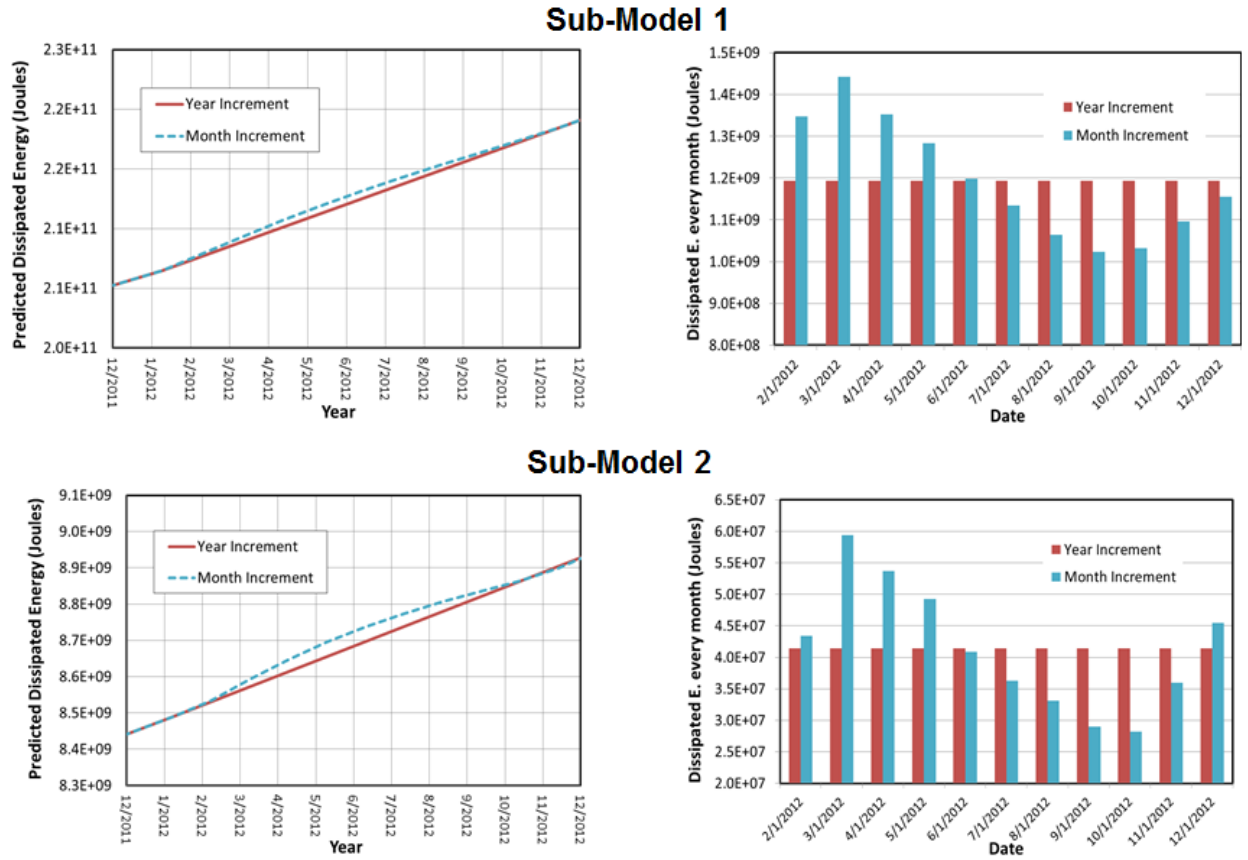


Figure 34: Comparison of the dissipated fault energy in geomechanics submodels 1 and 2. Faults are explicitly modeled and the month-to-month variation in slip can be observed. The difference in the total dissipated energy at the end of one year is negligible (<0.2%)

This result is to be expected given the physics that are captured in the static geomechanics model. The reservoir rocks are modeled as a linear elastic-perfectly plastic material. The stresses do not result in plastic deformation so the material response is linear elastic and there is no rate dependence. The only rate dependence in the static geomechanical model is the behavior of the salt that overlies the reservoir. The salt is modeled using a creep material model provided by NAM, but the effect of this creep on the year time scale is negligible. The constitutive relationship that governs the fault sliding (Coulomb frictional sliding with no cohesion) does not have a rate dependence so a rate dependent result should not occur. Under some loading conditions, frictional sliding is a history dependent process so areas that experience loading and unloading can show an effect, but based on the results of submodel 2, this effect is negligible.

4.1.3 Summary and Conclusions

The static geomechanics model shows a negligible change in the total dissipated energy if month-to-month variations in production are included. This result is expected given the assumptions on the physics that are captured by the static geomechanics model but it is consistent with the conclusion that the total observed seismicity should not change as a result of constant vs. variable production rates. Alternative models that capture rate and history dependence of frictional sliding processes (such as those presented in the previous section) need to be considered.

4.2 Surface Reservoir Water Level Fluctuations as an Analog

Seismicity is observed to occur after the impoundment of surface water reservoirs. The seismicity is a coupled poroelastic response to the change in overburden stress that results from large water level changes. The response depends on the frequency of lake-level changes, reservoir dimensions, and the geometry of faults surrounding the reservoir. In most cases surface reservoir induced seismicity occurs shortly after the impoundment. Seismicity is often observed to start at a high level and decay with time. However, seismicity can also start long after initial impoundment and can occur after large lake-level changes or if the reservoir is filled above the highest water level previously achieved

One example of surface reservoir induced seismicity is from Monticello, South Carolina USA. A high rate of earthquakes is observed immediately following impoundment and this decreases in time to pre-impoundment levels. In Monticello, seismicity decays to pre-fill levels, even in the presence of relatively small lake level fluctuations (~1.5 m) (Chen and Talwani, 2001).

In a few cases, seismicity continues for several years, and even decades after the initial impoundment. The best examples of this behavior are Lake Mead, USA (Rogers and Lee, 1976) and Koyna Reservoir, India (Pavan Kumar et al., 2012). Protracted seismicity can occur and/or continue with cyclical water level changes a significant fraction of the water depth.

Studies of surface water reservoirs are interesting because they are additional examples of seismic response to fluctuations in pore pressure and stress, but it is not clear how to translate these observations to conclusions about Groningen seismicity and changes in hazard due to fluctuations.

5.0 Summary and Conclusions

This document summarizes the studies performed by EMURC during 2015-2016 in an effort to determine the impact of fluctuations in production on the seismicity observed at Groningen. Work previously published on this subject by other entities has focused on the seasonality of earthquakes and whether high production during the winter months leads to more earthquakes in the winter and spring (Bierman et al., 2015 and Nepveu, et al., 2016). This study addresses whether the hazard is changed due to fluctuations in production by looking for evidence of a change in the character of the seismicity (more earthquakes or bigger earthquakes) when compared to steady production. Shifting earthquakes from the summer to the winter months does not change the hazard unless the number or magnitude of expected events throughout the year is changed. The model results presented here predict that there should be a seasonality to the earthquakes and the statistical model confirms that more events do occur during the winter and spring as a result of high winter production. However, the model results do not imply that there should be an increase in the hazard due to fluctuating production throughout the year and the statistical analysis agrees that there has not been an observable increase in the implied hazard associated with fluctuating production.

If fluctuations in production are to change the character of seismicity there must be a mechanism for faults to “feel” the effect of fluctuations in production. Therefore, the first study conducted by EMURC examined the effect of fluctuations in production on the stress state of faults at various distances from producing wells. The average pore pressure in the field is decreasing but localized areas in the vicinity of wellbores (within ~200 m) may experience pore pressure increases and decreases due to seasonal and daily fluctuations in production. However, the magnitudes of these fluctuations in pore pressure are very small ($\sim\pm 0.1$ bar) in comparison to the general level of reservoir depletion at Groningen, which is over 200 bar. Most faults in the field are far enough from wells that they aren’t materially affected by whether wells are producing at a constant rate or are fluctuating in production on short time scales. Due to the limited spatial extent and relatively small magnitude of the effect, it suggests that the effect of fluctuations in production should be small and the aggregate seismic hazard should be mostly dependent on the cumulative production/depletion.

However, even small differences in stress loading histories could have an effect on the resulting seismicity. Recent work focused on the development and use of a new geomechanical model to simulate earthquake catalogs by implementing a rate-and-state frictional description of the fault. This formulation is well suited to address the issue of production fluctuations because the “state” portion of the formulation makes the model result dependent on the sliding history of the fault and could allow for differences in behavior based on the production (or stress) history.

A simplified implementation considers only the earthquake occurrence rate and how it is affected by the stress history. This model was used to compare instantaneous earthquake rates and the total number of earthquakes for constant versus seasonal and daily fluctuations in shear stressing rate. The same number of earthquakes was found to occur in all the scenarios but the timing of the earthquakes was shifted within the time frame based on the loading history.

Recently this model was greatly expanded into a full rate-and-state fault friction representation where coseismic and interseismic times were modeled and the resulting earthquake catalogs (timing and magnitudes) were compared for different scenarios. Many model parameters and methods of implementation were examined and all models reached the same conclusion: there is no aggregate change in the character of the seismicity due to constant versus fluctuating production. Many catalogs are simulated under different loading histories and the results are examined in aggregate to determine if there is a statistically significant effect on the observed seismicity. Any individual model realization could lead the observer to conclude that one production scenario is “worse” than another, but when many model realizations are viewed in aggregate, there is no statistical difference between the scenarios. The modeled earthquake timing shifts within the year, but there is no change to the expected number of modeled events or magnitude of events within a year. Neither this model nor any other physical model examined to date suggests that fluctuations in production will alter the character of the seismicity and thus impact the aggregate seismic hazard.

The study shows that the production schedule affects the timing of earthquake events but neither suggest that the hazard is impacted by fluctuations in production schedule. For example, the model shows that if a given amount of gas is produced each year, shifting that production to the winter increases the number of events in the winter and spring, but statistically the same modeled number and magnitude of events occur during the year as if the production had been constant throughout the year. Therefore, since there is no change in the total number of modeled events or the expected magnitudes, there is no expected change in hazard for the year.

Multiple types of physics based models and a statistical analysis of the field data support the conclusion that fluctuations in gas production rate do not impact the aggregate seismic hazard compared to a steady production scenario. However, these results cannot eliminate the possibility that a link between fluctuations in production and increased seismic hazard could be found in the future. The analyses conducted by EMURC to date support the notion that Groningen gas production can be fluctuated as necessary (on a seasonal or daily basis), without exposing the Groningen area to a change in the aggregate seismic hazard so long as an offsetting change in production also occurs to balance the total production rate.

References

- Akaike, H. (1974), A new look at the statistical model identification, *IEEE Trans. Automat. Contr.*, 19, 716-723, doi:10.1109/TAC.1974.1100705.
- Bierman, S., R. Paleja, and M. Jones (2015), Statistical methodology to test for seasonal variation in rates of earthquakes in the Groningen field, NMI publication.
- Bourne, S. J., S. J. Oates, J. van Elk, and D. Doornhof (2014), A seismological model for earthquakes induced by fluid extraction from a subsurface reservoir, *J. Geophys. Res. Solid Earth*, 119, 8991-9015, doi:10.1002/2014JB011663.
- Bourne, Stephen and Oates, Steve (2014), An activity rate model of induced seismicity within the Groningen Field, NMI publication.
- Brodsky, E. E., and N. J. van der Elst (2014), The uses of dynamic earthquake triggering, *Ann. Rev. Earth Planet. Sci.*, 42, 317–339.
- Casella, G. and R. L. Berger (2001), *Statistical Inference*, 2nd ed., Duxbury Press.
- Chen, L., and P. Talwani (2001) Mechanism of Initial Seismicity Following Impoundment of the Monticello Reservoir, South Carolina, *Bull. Seis. Soc. Amer.*, 9(6) 1582-1594.
- Dempsey, D., and J. Suckale (2016), Collective properties of injection-induced earthquake sequences: 1. Model description and directivity bias, *J. Geophys. Res. Solid Earth*, 121, 3609–3637, doi:10.1002/2015JB012550.
- Dieterich, J. H. (1992), Earthquake nucleation on faults with rate-dependent and state-dependent strength, *Tectonophysics*, 211(1–4), 115–134.
- Dieterich, J. (1994), A constitutive law for rate of earthquake production and its application to earthquake clustering, *J. Geophys. Res.*, 99(B2), 2601–2618, doi:10.1029/93JB02581.
- Dieterich, J. H., and G. Conrad (1984), Effect of humidity on time- and velocity-dependent friction in rocks, *J. Geophys. Res.*, 89(B6), 4196–4202, doi:10.1029/JB089iB06p04196.
- Dieterich, J. H., K. B. Richards-Dinger and K. A. Kroll (2015), Modeling Injection-Induced Seismicity with the Physics-Based Earthquake Simulator RSQSim, *Seis. Res. Lett.*, 86(4), doi: 10.1785/0220150057.
- Di Toro, G., R. Han, T. Hirose, N. De Paola, S. Nielsen, K. Mizoguchi, F. Ferri, M. Cocco, and T. Shimamoto (2011), Fault Lubrication During Earthquakes, *Nature*, 471, 494-499
- Dost, B., F. Goutbeek, T. V. Eck, and D. Kraaijpoel (2012), Monitoring induced seismicity in the North of the Netherlands: Status report 2010, Tech. Rep., Royal Netherlands Meteorol. Inst., KNMI.

Efron, B. (1979), Bootstrap methods: Another look at the jackknife, *Ann. Statist.*, 7, 1-26, doi:10.1214/aos/1176344552.

Gardner, J.K. and Knopoff, L. (1974), Is the sequence of earthquakes in southern California, with aftershocks removed, Poissonian? *Bull. Seismol. Soc. Am.*, 64, 1363-1367.

Gutenberg, B., and C. Richter (1954), *Seismicity of the Earth and Associated Phenomena*, 2nd ed., Princeton Univ. Press, Princeton, N. J.

Kaneko, Y., J. P. Ampuero and N. Lapusta (2011), Spectral-element simulations of long-term fault slip: Effect of low-rigidity layers on earthquake-cycle dynamics, *J. Geophys. Res.*, 116, B10313, doi:10.1029/2011JB008395.

Kroll, K. A., K.B. Richards-Dinger, and J. H. Dieterich (2016), Effects of hydraulic Diffusivity and Rate- and State-Dependent Friction in Simulations of Injection Induced Seismicity, *Seismol. Soc. Amer. Annual Meeting*, April 2016, 87:2B, 480.

Lapusta, N., J. R. Rice, Y. Ben-Zion, and G. Zheng (2000), Elastodynamic analysis for slow tectonic loading with spontaneous rupture episodes on faults with rate- and state-dependent friction, *J. Geophys. Res.*, 105, 23,765–23,789.

Lele, S. P., S.-Y. Hsu, J. L. Garzon, N. DeDontney, K. H. Searles, G. A. Gist, and B. A. Dale (2016), Geomechanical Modeling to Evaluate Production-Induced Seismicity at Groningen Field, *Society of Petroleum Engineers*, November 7, 2016, doi:10.2118/183554-MS.

Liu, Y., and J. R. Rice (2007), Spontaneous and triggered aseismic deformation transients in a subduction fault model, *J. Geophys. Res.*, 112, B09404, doi:10.1029/2007JB004930.

Marone, C. (1998), Laboratory-Derived Friction Laws and Their Application to Seismic Faulting, *Ann. Rev. Earth Planet. Sci.*, 26, 643-696.

Marzocchi, W., and L. Sandri (2003), A review and new insights on the estimation of the b-value and its uncertainty, *Ann. Geophys.*, 46, 1271-1282.

Nelder, J. A., R. W. M. Wedderburn (1972), Generalized Linear Models, *J. R. Statist. Soc. A.*, 135, 370-384.

Nepveu, M., K. van Thienen-Visser, and D. Sijacic (2016), Statistics of seismic events at the Groningen field, *Bull Earthquake Eng.*, 14, 3343-3362.

Pavan Kumar, J., D.V. Ramana, R. K. Chadha, C. Singh, and M. Shekar (2012) The relation between Seismicity and Water Level Changes in the Koyna-Warna Region, India, *Nat. Hazards Earth Syst. Sci.*, 12 813-817.

Rice, J. R. (1993), Spatio-temporal complexity of slip on a fault, *J. Geophys. Res.*, 98(B6), 9885– 9907.

Rice, J. R., and Y. Ben-Zion (1996), Slip complexity in earthquake fault models, *Proc. Natl. Acad. Sci. U.S.A.*, 93, 3811 –3818.

Rogers, A. M., and W. H. K. Lee (1976) Seismic Study of Earthquakes in the Lake Mead, Nevada-Arizona Region, *Bull. Seis. Soc. Amer.*, 66(5), 1657-1681.

Ruina, A. (1983), Slip instability and state variable friction laws, *J. Geophys. Res.*, 88(Nb12), 359–370.

van der Elst, N. J., and H. M. Savage (2015), Frequency Dependence of Delayed and Instantaneous Triggering on Laboratory and Simulated Faults Governed by Rate-State Friction, *J. Geophys. Res. Solid Earth*, 120, 3406-3429, doi:10.1002/2014JB011611.

